

Analytical approach to the transient and steady-state Cyclic Voltammetry of non-reversible electrode processes. Defining the transition from macro to microelectrodes

J. Gonzalez^a, A. Molina^{a*}, F. Martinez-Ortiz^a, M. Lopez-Tenes^a, R. G. Compton^b

^a Departamento de Química Física, Facultad de Química, Regional Campus of International Excellence “Campus Mare Nostrum”, Universidad de Murcia, 30100 Murcia, Spain

^b Department of Chemistry, Physical and Theoretical Chemistry Laboratory, Oxford University, South Parks Road, Oxford OX1 3QZ, United Kingdom

* Corresponding author

Abstract

An explicit analytical easily programmable expression for the current-potential curves of electrode processes of any degree of reversibility in Cyclic Voltammetry (CV), valid for small spherical electrodes, is presented. From this solution a complete analysis of the most relevant parameters of the CV curves in terms of the electrode size and the scan rate is made, and the different influences of the kinetics of the electrode process clearly determined. Moreover, the evolution of the main characteristics of the voltammograms in the transition from macro- to micro-electrodes is described. A global expression for the rate constant collecting the influence of the kinetics in the complete range of electrode size from macro to nanoelectrodes is defined. Simple particular expressions covering different kinetic and geometric limits are presented. Methods for extracting kinetic parameters of the response are proposed.

Keywords

Cyclic Voltammetry, Non-reversible electrode process, Microelectrodes, Spherical electrodes
Analytical modelling

1. Introduction

Cyclic Voltammetry (CV) is probably the most used electrochemical technique. Among the different reasons for this is its ease-of-implementation in the laboratory, its low number of parameters to be adjusted (mainly the scan rate), and that its response is very sensitive to the nature of the electrode process [1-5]. Its major drawbacks are that even for simple charge transfer processes with solution soluble species, as in the case of a single charge transfer, no simple analytical expressions of the current for quasi-reversible or fully irreversible charge transfer processes are available for macroelectrodes (which correspond to electrodes with a characteristic dimension r_0 which fulfils $\sqrt{Dt}/r_0 < 0.1$, with D being the diffusion coefficient and t the experiment time), or for microelectrodes (i. e., $\sqrt{Dt}/r_0 > 0.1$) under transient conditions [1-4].

To date, a number of numerical approaches, based mainly on software packages (DigiSim, DigiElch, KISSA, Comsol Multiphysics..., among others [6-10]), allow the simulation of CV responses at different electrode geometries for different reaction mechanisms. Although the usefulness of these packages is immense, it should be noted that analytical treatments, when available, provide explicit closed form expressions from which particular and limiting cases can be obtained. Moreover, they allow the direct deduction of the key variables of the process, making it easy to propose methods for the determination of kinetic and thermodynamic parameters of the system.

Explicit solutions for a single charge transfer at several electrode geometries under transient conditions have been reported in the simpler case of Nernstian behavior [3, 11-15], although in many cases they remain mathematically complex and hard to use for non-specialists [12-15]. In the case of non-Nernstian electrode processes, only expressions for the stationary behavior corresponding to micro and nanoelectrodes for different electrode geometries have been reported and methods based on the variation of the electrode size and the scan rate have been proposed to carry out the kinetic analysis of the process [16-21].

The study of the influence of the irreversibility on non stationary voltammograms is more difficult since the effective irreversibility is the result of a combination of "macro" and "micro" effects [3, 4, 17, 20-22]. Thus, for example, for macroelectrodes the kinetic analysis in CV is based mostly on the variation of relevant parameters of the voltammograms with the scan rate (for example, the peak currents and peak potentials for the direct and reverse scans and its difference, see [1, 3, 4, 23]). When the electrode size becomes relevant the influence of the scan rate becomes more complex. Moreover, as the size of electrode decreases, the peak tends to disappear in such a way that the half wave potential of the direct scan becomes the most reliable parameter.

In this paper we present a simple, easily programmable analytical expression for the current of a charge transfer process of any degree of reversibility under transient conditions valid for micro and submicroelectrodes of spherical or hemispherical geometry. The spherical electrode has been the most widely studied from a theoretical point of view given that its description is easier and more "intuitive" than those corresponding to non-uniformly accessible electrodes (e. g., disc electrodes), while the current-potential response fully illustrates the effects of convergent diffusion [1-4] and, therefore, this electrode geometry can be considered a benchmark of most of the signals observed at microelectrodes of other geometries. From this solution, a definition is extracted for the global rate constant of the electrode process which collects all the kinetic influences and covers the complete range of electrode sizes from macro to nanoelectrodes. This solution allows us to develop a complete analysis of the most relevant parameters of the CV response in terms of the electrode size and the scan rate thus clearly determining the different influences of the kinetics of the electrode process. Moreover, it offers the possibility of carrying out the complete characterization of the process when a transient or steady state voltammogram is obtained. Indeed, by using this solution it has been found that there exists a range of electrode sizes for which the voltammograms are sigmoidal in shape but they have a transient nature.

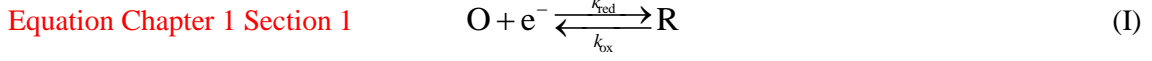
By combining the solution presented here and numerical calculations, a general scheme for the analysis of the CV curve, valid for any reversibility degree, is presented. Several transitions are indicated, showing the evolution of the main characteristics of the voltammograms from macroelectrodes to microelectrodes.

Simple expressions covering different kinetic and geometric limits are presented, and the validity of different methods used for extracting kinetic parameters of the response is checked.

2. Theory

2.1. Linear Sweep Voltammetry and Cyclic Voltammetry

Let us consider a one-electron reduction that takes place at a spherical or hemispherical electrode of radius r_s



where k_{red} and k_{ox} are the potential dependent heterogeneous rate constants for the electro-reduction and electro-oxidation processes, respectively.

By applying the procedure detailed in Appendix A, an expression for the current has been deduced (see Eq. (A43)), which is valid for an arbitrary sequence of potential pulses applied (i. e., for any potential pulse electrochemical technique) and any degree of reversibility of the charge transfer process. Moreover, this expression is independent of the kinetic model for the charge transfer, and can thus be applied when either the Butler-Volmer (BV) or Marcus-Hush (MH) models are chosen [3, 4, 24].

In this paper it will be considered the application of this general solution to a staircase potential perturbation with steps $E_1, E_2, \dots, E_j, \dots, E_p$ of duration τ such that:

$$\left. \begin{aligned} E_j &= E_{\text{initial}} - j\Delta E & \text{for } j = 1, 2, \dots, (p/2) \\ E_j &= E_{\text{final}} + (j - p/2)\Delta E & \text{for } j = (p/2) + 1, \dots, p \end{aligned} \right\} \quad (1)$$

with ΔE being the step size. In the case of Linear Sweep Voltammetry (LSV) and Cyclic Voltammetry (CV) the step size in Eq. (1) becomes very small for a fixed scan rate ($= \Delta E / \tau$), which in practice means that $\Delta E \leq 0.01$ mV, see [3, 11, 25]. So, the applied potential waveform given by Eq. (1) behaves in an analogous way to the following continuous function of time [1, 3]:

$$\left. \begin{aligned} E(t) &= E_{\text{initial}} - vt & \text{for } t \leq t_{\text{inv}} \\ E(t) &= E_{\text{final}} + v(t - t_{\text{inv}}) & \text{for } t > t_{\text{inv}} \end{aligned} \right\} \quad (2)$$

where t_{inv} is the time at which the scan is reversed and $v = dE / dt$.

In the following, the BV kinetics model will be considered. The results obtained with this theory can be also applied if MH formalism is considered since, in agreement with references [24, 26, 27], no significant differences between BV and MH models are observed unless extremely small electrodes or very low reorganization energies are considered [24, 28].

Under these conditions, the expression of the surface (denoted with the superscript "s") concentration of species O corresponding to the j -th potential pulse applied is (see Eq. (A40))

$$\frac{c_{\text{O}}^{(s,j)}}{c_{\text{O}}^*} = \frac{\prod_{l=1}^j (1 + k_{\text{T,CV}}^{l-1,l})}{\prod_{l=1}^j (1 + k_{\text{T,CV}}^{l,l})} + \sum_{l=1}^j \left(\left(k_{\text{ox,CV}}^{l,l} - k_{\text{ox,CV}}^{l-1,l} \right) \frac{\prod_{m=l}^{j-1} (1 + k_{\text{T,CV}}^{m,m+1})}{\prod_{m=l}^j (1 + k_{\text{T,CV}}^{m,m})} \right) \quad (3)$$

with

$$\left. \begin{aligned} k_{\text{ox,CV}}^{h,i} &= k_{\text{ox,CV}}^h \Delta_{\text{s,CV}}^i(\xi_s, \mathcal{G}_{i,j}) \\ k_{\text{red,CV}}^{h,i} &= k_{\text{red,CV}}^h \Delta_{\text{s,CV}}^i(\xi_s, \mathcal{G}_{i,j}) \end{aligned} \right\} \quad h, i=1, 2, \dots, j \quad (4)$$

$$k_{\text{T,CV}}^{h,i} = k_{\text{T,CV}}^h \Delta_{\text{s,CV}}^i(\xi_s, \mathcal{G}_{i,j}) = k_{\text{red,CV}}^{h,i} + k_{\text{ox,CV}}^{h,i} \quad h, i=1, 2, \dots, j \quad (5)$$

$$\left. \begin{aligned} k_{\text{red,CV}}^h &= k_d^0 e^{-\alpha \eta_h} \\ k_{\text{ox,CV}}^h &= k_{\text{red,CV}}^h e^{\eta_h} \\ k_{\text{T,CV}}^h &= k_{\text{red,CV}}^h + k_{\text{ox,CV}}^h \end{aligned} \right\} \quad h=1, 2, \dots, j \quad (6)$$

$$k_d^0 = \frac{k^0}{\sqrt{aD}(1+\xi_s)} \quad (7)$$

$$\eta_h = F(E_h - E_c^{0'})/RT \quad h=1, 2, \dots, j \quad (8)$$

$$\Delta_{\text{s,CV}}^i(\xi_s, \mathcal{G}_{i,j}) = \frac{1+\xi_s}{\xi_s + \frac{1}{\sqrt{\pi \mathcal{G}_{i,j}}}} \quad i=1, 2, \dots, j \quad (9)$$

$$\mathcal{G}_{i,j} = \frac{F}{RT} |E_{j-i+1} - E_{\text{initial}}| = at_{i,j} \quad i=1, 2, \dots, j \quad (10)$$

$$\xi_s = \frac{1}{r_s} \sqrt{\frac{D}{a}} \quad (11)$$

$$a = \frac{Fv}{RT} \quad (12)$$

and $k_{\text{T,CV}}^{0,1} = k_{\text{ox,CV}}^{0,1} = 0$.

$E_c^{0'}$ is the formal potential of the redox couple, k^0 is the standard heterogeneous rate constant and α is the charge transfer coefficient [29, 30]. $t_{i,j}$ is given by Eq. (A37).

The expression of k_d^0 given by Eq. (7) shows that the dimensionless rate constant is the product of two factors ($k_d^0 = (k^0 / \sqrt{aD}) \times (1 / (1 + \xi_s))$), with each collecting different influences on the global kinetics. The nature of each factor is discussed in section 2.1.2.

From Eq. (A43), the following explicit expression for the transient dimensionless CV current is obtained

$$\Psi^j = k_{\text{T,CV}}^j \left\{ \frac{\prod_{l=1}^j (1 + k_{\text{T,CV}}^{l-1,l})}{\prod_{l=1}^j (1 + k_{\text{T,CV}}^{l,l})} + \sum_{l=1}^j \left(k_{\text{ox,CV}}^{l,l} - k_{\text{ox,CV}}^{l-1,l} \right) \frac{\prod_{m=l}^{j-1} (1 + k_{\text{T,CV}}^{m,m+1})}{\prod_{m=l}^j (1 + k_{\text{T,CV}}^{m,m})} \right\} - k_{\text{ox,CV}}^j \quad (13)$$

with

$$\Psi^j = \frac{I^j}{FA_s c_O^* \sqrt{aD} (1 + \xi_s)} \quad (14)$$

Note that the dimensionless form of the CV current given by Eq. (14) is not the usual one ($\Psi^j = I^j / (FA_s c_O^* \sqrt{aD})$) [1, 3, 4, 23]. The additional term $(1 + \xi_s)$ has been included in this case in order to incorporate the effect of the electrode size (and, in practice, it only affects the magnitude of the current since ξ_s is independent of the applied potential, see Eq. (11)).

2.1.1. Reversibility limits

2.1.1.a Fully irreversible process

In this case the condition $k_{\text{red,CV}}^h \gg k_{\text{ox,CV}}^h$ can be assumed over the entire range of potentials of the experiment in such a way that Eqs. (3) and (13) lead us to the following simpler expressions of the surface concentrations and currents, respectively,

$$\frac{c_{\text{O,irrev}}^{(s,j)}}{c_O^*} = \frac{\prod_{l=1}^j (1 + k_{\text{red,CV}}^{l-1,l})}{\prod_{l=1}^j (1 + k_{\text{red,CV}}^{l,l})} \quad (15)$$

$$\Psi_{\text{irrev}}^j = k_{\text{red,CV}}^j \frac{\prod_{l=1}^j (1 + k_{\text{red,CV}}^{l-1,l})}{\prod_{l=1}^j (1 + k_{\text{red,CV}}^{l,l})} \quad (16)$$

2.1.1.b Reversible process

For high enough values of the rate constants (i. e., $k_{\text{red,CV}}^h \rightarrow \infty$ and $k_{\text{ox,CV}}^h \rightarrow \infty$), the expressions of the surface concentrations simplify greatly. By taking into account Eqs. (3) and (A38) of Appendix A, the following expressions for the surface concentrations and the current are obtained:

$$\frac{c_{\text{O,rev}}^{(s,j)}}{c_O^*} = \frac{e^{\eta_j}}{1 + e^{\eta_j}} \quad (17)$$

$$\Psi_{\text{rev}}^j = \sum_{l=1}^j Z_l / \Delta_{\text{s,CV}}^l (\xi_s, g_{l,j}) \quad (18)$$

with

$$Z_l = \begin{cases} \frac{1}{1 + e^{\eta_l}} & l = 1 \\ \frac{1}{1 + e^{\eta_l}} - \frac{1}{1 + e^{\eta_{l-1}}} & l \geq 2 \end{cases} \quad (19)$$

Equation (18) is the exact solution for the CV current of a Nernstian charge transfer process taking place at a spherical or hemispherical electrode (see for example Eq. (5.62) in [3]).

2.1.2. Geometrical limits

2.1.2.a. Macroelectrodes

By making $r_s \rightarrow \infty$ (i. e., $\xi_s \rightarrow 0$) in Eqs. (7) and (9), the expressions for k_d^0 and $\Delta_{s,CV}^i$ become

$$k_d^0(\xi_s \rightarrow 0) = \frac{k^0}{\sqrt{aD}} = k_{d,macro}^0 \quad (20)$$

$$\Delta_{s,CV}^i(\xi_s \rightarrow 0, \mathcal{G}_{i,j}) = \Delta_{macro,CV}^i(\mathcal{G}_{i,j}) = \sqrt{\pi \mathcal{G}_{i,j}} \quad (21)$$

Under these conditions the surface concentration of species O and the dimensionless current are given respectively by (see Eqs. (3) and (13))

$$\frac{c_{O,macro}^{(s,j)}}{c_O^*} = \frac{\prod_{l=1}^j (1 + k_{T,CV,macro}^{l-1,l})}{\prod_{l=1}^j (1 + k_{T,CV,macro}^{l,l})} + \sum_{l=1}^j \left(k_{ox,CV,macro}^{l,l} - k_{ox,CV,macro}^{l-1,l} \right) \frac{\prod_{m=l}^{j-1} (1 + k_{T,CV,macro}^{m,m+1})}{\prod_{m=l}^j (1 + k_{T,CV,macro}^{m,m})} \quad (22)$$

$$\Psi_{macro}^j = k_{T,CV,macro}^j \left\{ \frac{\prod_{l=1}^j (1 + k_{T,CV,macro}^{l-1,l})}{\prod_{l=1}^j (1 + k_{T,CV,macro}^{l,l})} + \sum_{l=1}^j \left(k_{ox,CV,macro}^{l,l} - k_{ox,CV,macro}^{l-1,l} \right) \frac{\prod_{m=l}^{j-1} (1 + k_{T,CV,macro}^{m,m+1})}{\prod_{m=l}^j (1 + k_{T,CV,macro}^{m,m})} \right\} - k_{ox,CV,macro}^j \quad (23)$$

with

$$\left. \begin{aligned} k_{ox,CV,macro}^{h,i} &= k_{ox,CV}^h \Delta_{macro,CV}^i(\mathcal{G}_{i,h}) \\ k_{red,CV,macro}^{h,i} &= k_{red,CV}^h \Delta_{macro,CV}^i(\mathcal{G}_{i,h}) \\ k_{T,CV,macro}^{h,i} &= k_{red,CV,macro}^{h,i} + k_{ox,CV,macro}^{h,i} \end{aligned} \right\} \quad h, i=1, 2, \dots, j \quad (24)$$

and $k_{red,CV}^h$ and $k_{ox,CV}^h$ given by Eq. (6) by changing k_d^0 by $k_{d,macro}^0$.

Eq. (20) shows that for macroelectrodes the dimensionless rate constant k_d^0 is reduced to a "macro" term and any geometrical influence is lost since a macroelectrode is not sensitive to its geometry.

2.1.2.b. Microelectrodes.

For microelectrodes, condition $\xi_s \gg 1$ holds and, therefore (see Eqs. (7) and (9)),

$$k_d^0(\xi_s \gg 1) = k_{d,ss}^0 = \frac{k_{d,macro}^0}{\xi_s} = \frac{k_s^0 r_s}{D} \quad (25)$$

$$\Delta_{s,CV}^i(\xi_s \gg 1, \mathcal{G}_{i,j}) \cong \Delta_{ss,CV} = 1 \quad (26)$$

By inserting Eqs. (25) and (26) into Eqs. (3) and (13), the surface concentration of species O and the dimensionless current, respectively, simplify to

$$\frac{c_{O,ss}^{(s)}}{c_O^*} = \frac{1 + k_{ox,ss}}{1 + k_{T,ss}} \quad (27)$$

$$\Psi_{ss} = \frac{k_{red,ss}}{1 + k_{T,ss}} \quad (28)$$

with

$$\left. \begin{aligned} k_{red,ss} &= k_{d,ss}^0 e^{-\alpha\eta} \\ k_{ox,ss} &= k_{red,ss} e^{\eta} \\ k_{T,ss} &= k_{red,ss} + k_{ox,ss} \end{aligned} \right\} \quad (29)$$

and $\eta = F(E - E_c^{0'})/RT$

Note that it is possible to re-write Eq. (28) in terms of the real current by inserting Eqs. (14), (25) and (29):

$$\frac{I_{ss}}{I_{d,ss}} = \frac{k_{d,ss}^0 e^{-\alpha\eta}}{1 + k_{d,ss}^0 e^{-\alpha\eta} (1 + e^{\eta})} \quad (30)$$

with

$$I_{d,ss} = FA_s c_O^* \sqrt{aD} \xi_s = FA_s c_O^* D \frac{1}{r_s} \quad (31)$$

Eq. (30) corresponds to the well known expression for the steady state current of a non-reversible charge transfer at a spherical electrode (see for example Eq. (25) in [19] or [1, 3, 4, 11, 13]).

Note also that it is possible to rewrite Eq. (30) as

$$\frac{1}{I_{ss}} = \frac{1}{I_{d,ss}} + \frac{1}{I_{d,ss} k_{red,ss}} + \frac{1}{I_{d,ss} e^{-\eta}} \quad (32)$$

with the first term on the right hand side being related to the electrode size, and the second one providing a kinetically controlled contribution to the current. Eq. (32) agrees with that deduced by Oldham [16, 22, 31].

Under these conditions, the dimensionless voltammogram given by Eq. (28) presents a sigmoidal feature with a current plateau equal to the unity. The value of the half-wave potential, $E_{1/2}$, can be obtained from the following implicit equation,

$$e^{-\alpha\eta_{1/2}}(1 - e^{\eta_{1/2}}) = \frac{1}{k_{d,ss}^0} \quad (33)$$

with $\eta_{1/2} = F(E_{1/2} - E_c^{0'})/RT$. Eq. (33) leads to two limiting expressions corresponding to reversible and fully irreversible processes (with a maximum error of 5 mV),

$$E_{1/2,rev} = E_c^{0'} \quad \log(k_{d,ss}^0) \geq 1.3 \quad (34)$$

$$\begin{aligned} E_{1/2,irrev} &= E_c^{0'} + \frac{RT}{\alpha F} \ln(k_{d,ss}^0) = \\ &= E_c^{0'} + \frac{RT}{\alpha F} \ln\left(\frac{k^0}{D}\right) + \frac{RT}{\alpha F} \ln(r_s) \quad \log(k_{d,ss}^0) \leq -0.57 \end{aligned} \quad (35)$$

General Eq. (13) becomes Eq. (28) for $\log(\xi_s) \geq 1.2$ with errors below 5% (see section 3.3). It is important to emphasise that, for values of $\log(\xi_s) < 1.2$, sigmoidal CV curves with a transient character can be obtained. Due to this transient nature, these voltammograms should be analysed with the general Eq. (13). For a quantitative discussion on this point see section 3.3.

2.1.3. Diffusion layer thickness for non-Nernstian processes

A useful parameter for analysing the nature of the electrode process and the influence of the diffusion field on the response is the diffusion layer thickness, δ , which has usually been defined for the application of a single constant potential in fast and slow charge transfer processes [1, 3, 4, 32-35], but it can also be defined for any potential E_j of a given potential waveform [3, 33]. In the case of CV, it takes the form

$$\delta_{CV} = \frac{\Delta c_O^j}{\left(\partial c_O^j / \partial r\right)_{r_s}} = \frac{c_O^* - c_O^{(s,j)}}{I^j / (FA_s D)} = \frac{1 - \left(c_O^{(s,j)} / c_O^*\right)}{\Psi^j} \sqrt{\frac{D}{a}} \frac{1}{1 + \xi_s} \quad (36)$$

with $\Delta c_O^j = c_O^* - c_O^{(s,j)}$, and $c_O^{(s,j)}$ and Ψ^j given by Eqs. (3) and (13), respectively.

From Eq. (36) it can be deduced that the diffusion layer thickness is, in general, a growing function of the negative applied potential, especially in the case of macroelectrodes (for a more detailed discussion see [33]). The following expression for the diffusion layer thickness is obtained for steady-state current-potential curves at microelectrodes, by inserting Eqs. (27)-(28) into (36)

$$\delta_{CV,ss} = \frac{1}{\xi_s} \sqrt{\frac{D}{a}} = r_s \quad (37)$$

Thus, under these conditions, $\delta_{CV,ss}$ remains constant for all the potential scan [33].

3. Results and Discussion

3.1. General behavior of the CV curves

The validity of the analytical solution for the current given in Eq. (13) was checked by comparison with numerical calculations (see Appendix B). Very good agreement between analytical and numerical results was found for the half-peak potential, $E_{1/2,p}$, or the half-wave potential $E_{1/2}$ when the response is sigmoidal, of the direct scan, whatever the electrode size considered, including macroelectrodes (with maximum differences of 10 mV for fully irreversible processes at macroelectrodes). Moreover, the error in the peak or plateau currents (when the response is sigmoidal) calculated with Eq. (13) is less than 5% for $\log(\xi_s (= \sqrt{D/a} / r_s)) \geq -0.4$ whatever the degree of reversibility of the process. Below this $\log(\xi_s)$ value, the error increases until it reaches a maximum value of 23% for fully irreversible processes at macroelectrodes. These higher differences are related to a better behavior of the analytical solution proposed for small electrodes (for a detailed numerical quantitative analysis of the peak heights and potentials in terms of the electrode size see Appendix B).

The global behavior of the voltammograms is controlled by two key dimensionless parameters, $k_{d,macro}^0$ (Eq. (20)) and ξ_s (Eq. (11)), and $k_d^0 (= k_{d,macro}^0 / (1 + \xi_s))$ can be considered as an "effective" rate constant which contains the kinetic influence of the charge transfer process by incorporating both "macro" irreversibility (through the dimensionless rate constant $k_{d,macro}^0$) and "micro" irreversibility (through the term related with electrode size, $1/(1 + \xi_s)$). This behavior can be seen in Fig. 1, where the evolution of $\log(k_d^0 / k_{d,macro}^0)$ has been plotted versus $\log(\xi_s)$. Thus, $k_d^0 = k_{d,macro}^0$ for $\log(\xi_s) \leq -1.64$ with errors below 1% (zone I in this Figure). The "effective" rate constant decreases when ξ_s increases (see zone II) until it reaches the value $k_d^0 = k_{d,ss}^0$ for $\log(\xi_s) \geq 1.47$, with errors below 1% (zone III).

< Figure 1 >

From a practical point of view, two experimental variables - the scan rate and the electrode radius - are decisive in controlling the behavior shown in Fig. 1. The influence exerted by the scan rate on the kinetics of the CV curves for spherical electrodes is complex since it affects both k_d^0 and ξ_s (see Eqs. (7) and (11), respectively). Indeed, the expression of k_d^0 can be rewritten as

$$k_d^0 = \frac{k^0}{\sqrt{aD} + \frac{D}{r_s}} \quad (38)$$

Thus, an increase of the scan rate implies that $k_d^0 \rightarrow k_{d,macro}^0$ (zone I in Fig. 1). Otherwise, the decrease of "a" causes the opposite effect and therefore $k_d^0 \rightarrow k_{d,ss}^0$ (zone III in Fig. 1), which means that the overall rate constant suffers a decrease in relation to $k_{d,macro}^0$.

In the following, we will use the dimensionless current defined in Eq. (14) in order to simplify the behavior of the voltammograms. Note that this normalization can be easily performed from experimental data.

Figures 2 and 3 account for the influence of ξ_s on the dimensionless current-potential response, $\Psi - \eta$ curves (Figs. a), the dimensionless linear diffusion layer thickness $\delta_N = \delta_{CV}(1 + \xi_s) / (\sqrt{D/a})$ (Figs. b), and the surface concentration of oxidised species $c_O^{(s,j)} / c_O^*$ (Figs. c), calculated from Eqs. (13), (36) and (3), respectively. These curves have been obtained for $k_{d,macro}^0 = 1$ (Figure 2) and $k_{d,macro}^0 = 10^{-2}$ (Figure 3), and $\alpha = 0.5$.

< Figures 2-3 >

As can be seen in Figs. 2a and 3a, the decrease of $k_{d,macro}^0$ leads to a decrease of the peak current which is much more marked in the peak corresponding to the reverse scan (see also Fig. B1), together with an increasing separation of the direct and reverse curves, which is much more evident as ξ_s increases. An increase of ξ_s leads to the evolution of the voltammograms from a peak shaped feature to a sigmoidal one (see curves with $\xi_s \geq 5$). In practice, obtaining a sigmoidal current-potential curve depends on ξ_s and $k_{d,macro}^0$ and, for a given value of $k_{d,macro}^0$, ξ_s must be greater than a limit value, which will be denoted as $\xi_{s,lim}$. In this work it is assumed that the voltammogram is sigmoidal when the relative difference between the maximum current and that obtained at a potential 300 mV more negative is below 5%. Under these conditions the peak current is no longer a relevant parameter for a quantitative kinetic analysis and the plateau current and the half-wave potential of the direct scan are now the parameters to determine.

It can be also seen from Figs. 2a and 3a that the rise of ξ_s leads to a shift of the cathodic response towards more negative potentials (this shift in terms of half-peak or half-wave potential is around 130 mV for $k_{d,macro}^0 = 1$ and of 185 mV for $k_{d,macro}^0 = 10^{-2}$ when ξ_s changes from 0.1 to 10). This higher sensitivity of the voltammograms of microelectrodes to the kinetics is well known, and is attributed to a faster mass transport which augments the influence of the "micro" irreversibility on the overall kinetics [1, 3, 4, 22, 31].

The normalised linear diffusion layer thickness δ_N shown in Figs. 2b and 3b is, in general, a growing function of the negative applied potential, more marked in the case of macroelectrodes, although it tends to a constant value at very positive potentials, showing the following limiting values independently of the electrode kinetics,

$$\left. \begin{aligned} \delta_N|_{E \gg E_c^{0'}} &= 1 & (a) \\ \delta_N|_{E \ll E_c^{0'}} &= \frac{1 + \xi_s}{\frac{1}{\sqrt{\pi\eta}} + \xi_s} & (b) \end{aligned} \right\} \quad (39)$$

with $\eta = F(E - E_c^{0'}) / RT$. The anodic limit is reached for $\eta \geq 10$ when $k_{d,macro}^0 = 1$ and $\eta \geq 20$ in the case of $k_{d,macro}^0 = 10^{-2}$, whereas the cathodic one is reached for $\eta \leq -17.3$ when $k_{d,macro}^0 = 1$ and $\eta \leq -25$ in the case of $k_{d,macro}^0 = 10^{-2}$.

For microelectrodes ($\xi_s > 5$), a constant value of δ_N (equal to the unity) is observed for any value of the potential, which is characteristic of a steady state response [33]. For a given value of ξ_s , the normalised diffusion layer thickness δ_N deviates from this value at more positive potentials the more irreversible the process is, revealing a lesser ability of the irreversible current-potential curve to attain a stationary character.

Regarding the evolution of the surface concentrations with the potential, it can be seen that for high values of $k_{d,macro}^0$ or ξ_s (Figs. 2c and 3c) they are practically coincident for the direct and reverse scans, due to the fulfilment of Eqs. (17) (curves with $k_{d,macro}^0 = 1$, Fig. 2c), (27) (curves with $\xi_s > 1$ in Fig. 3c) and (A31), which indicates that the value of $c_O^{(s,j)}$ depends only on the last potential applied and that it has lost the memory of the previous pulses. When fully irreversible processes take place, increasing differences are observed between $c_O^{(s,j)}$ values during the direct and reverse scans, which are indicative of the transient nature of the response with a growing influence of the previous pulses, and are more evident in the case of macroelectrodes for which $c_O^{(s,j)}$ is given in an approximate way by Eq. (22) (see curves with $k_{d,macro}^0 = 10^{-2}$ and $\xi_s = 0.1$ in Fig. 3c).

3.2. Reversibility criteria

The expression for the anodic limit of the diffusion layer thickness allows us to introduce a general reversibility criterion, albeit approximate, for the CV responses at spherical

electrodes. In agreement with references [1, 3, 4, 36], this criterion is based on the ratio R between the standard heterogeneous rate constant, k^0 , and the mass transport coefficient, m_{CV} ($= D / \delta_{CV}$) [3]. Under CV conditions, the usual way of deducing this relationship is to consider the value of m_{CV} when $E \gg E_c^{0'}$, i. e., when the charge transfer process does not occur. In this case, the diffusion layer thickness is independent of the reversibility of the process and takes the limiting value given in Eq. (39), which can be written as

$$\delta_{CV}|_{E \gg E_c^{0'}} = \frac{1}{1 + \xi_s} \sqrt{\frac{D}{a}} \quad (40)$$

and therefore

$$R = \frac{k^0}{m_{CV}} = \frac{k^0 \delta_{CV}|_{E \gg E_c^{0'}}}{D} = \frac{k^0}{\sqrt{Da}} \frac{1}{1 + \xi_s} = k_{d,macro}^0 \frac{1}{1 + \xi_s} = k_d^0 \quad (41)$$

This ratio confirms the validity of the dimensionless rate constant, k_d^0 , for analysing the global kinetics influence on the CV curves. In agreement with [3], the following approximate values have been suggested for delimiting the kinetic regions of a single charge transfer,

$$\left. \begin{array}{ll} k_d^0 \geq 10 & \text{reversible process} \\ 10 > k_d^0 \geq 0.05 & \text{quasi-reversible process} \\ k_d^0 < 0.05 & \text{fully irreversible process} \end{array} \right\} \quad (42)$$

3.3. Analysis of the characteristic parameters of the cyclic voltammograms

Figure 4 shows the evolution of the peak current, Ψ_{peak} , and half-peak potentials, $\eta_{p/2}$, or the plateau current, $\Psi_{plateau}$, and half-wave potentials, $\eta_{1/2}$ (when a sigmoidal response is obtained), of the dimensionless voltammograms, plotted as a function of $\log(k_{d,macro}^0)$ and $\log(\xi_s)$ in a 3D scheme. Moreover, in Figs. 5 and 6 we have plotted the evolution of these parameters as a function of $\log(k_{d,macro}^0)$ for fixed ξ_s values (Fig. 5), and as a function of $\log(\xi_s)$ for fixed $k_{d,macro}^0$ values (Fig. 6). These figures provide a whole picture of the kinetics influences on the dimensionless voltammograms.

We have marked the values of k_d^0 which separate the Reversible, Quasi-Reversible and Fully Irreversible zones (blue circles lines, see Eqs. (7) and (42)) on the 3D surfaces of Fig. 4 and also in Fig. 5. In the following, a brief discussion of the most relevant aspects of the peak / plateau currents and half-peak / half-wave potentials is given.

< Figures 4-6 >

3.3.A. *Peak / Plateau currents*

On the basis of the results plotted in Figs. 4-6, different regions can be delimited for the behavior of the CV curves as a function of $\log(\xi_s)$, as shown in Scheme I.

- Zone a, $\log(\xi_s) \leq -1.3$, macroelectrode behavior (i. e., planar behavior). In this zone the dimensionless current is independent of the geometry. Due to the approximate results provided by Eq. (23) for the peak currents, numerical calculations have been performed.
- Zone b, $-1.3 < \log(\xi_s) \leq -1.1$. In this zone the transition from macro to spherical electrodes occurs and the electrode geometry must be considered for $\log(\xi_s) > -1.3$ for fully irreversible processes (FI) and for $\log(\xi_s) > -1.1$ for reversible ones (R).
- Zone c, $-1.1 < \log(\xi_s) \leq 0.04$. Transient peak-shaped curves for spherical electrodes, independently of the reversibility of the process, are obtained. For $\log(\xi_s) > -0.4$ Eq. (13) is valid.
- Zone d, $0.04 < \log(\xi_s) \leq 0.32$. Transition from transient peak-shaped to transient sigmoidal shaped CV curves which corresponds to $\log(\xi_s) > 0.04$ for fully irreversible processes and to $\log(\xi_s) > 0.32$ for reversible ones.
- Zone e, $0.32 < \log(\xi_s) \leq 1.2$, transient sigmoidal CV curves, which are scan rate dependent and show no superposition between the currents of the direct and reverse scans, for any degree of reversibility.
- Zone f, $\log(\xi_s) > 1.2$. The sigmoidal CV curves present a steady-state nature, which are scan rate independent (i. e., superimposable currents for the direct and reverse scans independently of the electrode kinetics). The expression of the current is given by Eq. (28).

< Scheme I >

The higher variation of the peak currents with $\log(k_{d,macro}^0)$ is observed at macroelectrodes (see Figs. 4, 5a and 6a for $\log(\xi_s) \leq -1.1$), with Ψ_{peak} taking the well known value of 0.446 for $\log(k_{d,macro}^0) \geq 1.5$ [1, 3, 4]. Otherwise, for $\log(\xi_s) \geq 0.25$ the plateau current is barely sensitive to the kinetics, with differences below 5% in the values of the maximum current, and it becomes independent of $k_{d,macro}^0$ for $\log(\xi_s) \geq 1.2$ since under these conditions (zone f in Scheme I, see Eq. (28))

$$\Psi_{ss}^{plateau} \cong 1 \quad (43)$$

According to Eq. (43), the difference between a stationary dimensionless sigmoidal curve and a transient sigmoidal one can be measured from the difference $(1 - \Psi^{plateau})$. Fig. 7

shows the $\Psi - \eta$ curves obtained for several values of $\log(k_{d,macro}^0)$ (shown on the curves), under steady state conditions (Eq. (28)) and also calculated for different values of $\log(\xi_{s,lim})$ from which a sigmoidal current is obtained. Thus, for example, for a reversible process with $\log(k_{d,macro}^0) = 2$ and $\log(\xi_{s,lim}) = 2.11$, $(1 - \Psi^{plateau}) = (1 - 0.763) = 0.237$ whereas for a fully irreversible one with $\log(k_{d,macro}^0) \leq -1$ and $\log(\xi_{s,lim}) = 1.09$, this difference is $(1 - 0.621) = 0.379$. These results indicate again the greater difficulty of non-reversible electrode processes in attaining a true stationary state [3, 17, 31].

3.3.B. Half-peak / Half-wave potentials

In the case of macroelectrodes, expressions for the half-peak potential have been reported for Nernstian and fully irreversible processes [1, 3, 4, 36]:

$$E_{p/2} = \begin{cases} E_c^{0'} + 1.09 \frac{RT}{F} & \text{reversible} \\ E_c^{0'} + \frac{RT}{\alpha F} \ln \left(2.936 \frac{k_{d,macro}^0}{\sqrt{\alpha}} \right) & \text{fully irreversible} \end{cases} \quad (44)$$

These values are marked with dotted lines in Fig. 5b. As $k_{d,macro}^0$ decreases, the half-peak or half-wave potential of the direct scan deviates more from the value corresponding to a reversible process the smaller the electrode size, showing a linear dependence with $\log(k_{d,macro}^0)$ for fully irreversible processes (see Fig. 5b). In the particular case of microelectrodes for fully irreversible processes, the half peak potential becomes (see Eq. (35)),

$$E_{1/2} = E_c^{0'} + \frac{RT}{\alpha F} \ln(k_{d,ss}^0) = E_c^{0'} + \frac{RT}{\alpha F} \ln \left(\frac{k_{d,macro}^0}{\xi_s} \right) = E_c^{0'} + \frac{RT}{\alpha F} \ln(k_{d,macro}^0) - \frac{RT}{\alpha F} \ln(\xi_s) \quad (45)$$

A similar behavior has been found for disc microelectrodes [16, 31]. This expression explains the linear zones observed in the fully irreversible region for the half-wave potential with $\log(k_{d,macro}^0)$ (Fig. 5b) and with $\log(\xi_s)$ (Fig. 6b). The limiting value of ξ_s to ensure the fulfilment of Eq. (45) with a 5% error is $\log(\xi_s) \geq 0.92$ for $\log(k_{d,macro}^0) \leq 0$ (see dotted vertical line in Fig. 6c). In agreement with this Equation, as is well known, the plots of the half-wave potential versus the logarithm of the electrode radius can be used to determine the rate constant and the charge transfer coefficient (see Eq. (35) and [18-20]).

Scheme II summarises the zones of applicability of Eqs. (44) and (45) for the half-peak / half-wave potential of the direct scan in terms of $\log(\xi_s)$. Note that the expression for $E_{p/2}$ for

Nernstian processes ($\log(k_{d,\text{macro}}^0) > 1$) can be used even for spherical electrodes up to $\log(\xi_s) \leq -0.7$. In practice, for $D = 10^{-5} \text{ cm}^2 \text{ s}^{-1}$ and $\nu = 0.1 \text{ V s}^{-1}$, this means that electrode radii up to $80 \text{ }\mu\text{m}$ can be used.

For $-0.7 \leq \log(\xi_s) \leq 0.92$ no linear dependence is observed between $E_{p/2}$ or $E_{1/2}$ and $\log(\xi_s)$ whatever the reversibility.

Under pure stationary conditions ($\log(\xi_s) \geq 1.2$), another typically used approach to analyse the fully irreversible current-potential curves is based on the following relationships (see Eq. (28))

$$E = E_{1/2,\text{irrev}} - \frac{RT}{\alpha F} \ln \left(\frac{\Psi_{ss}}{\Psi_{ss}^{\text{plateau}} - \Psi_{ss}} \right) \quad (46)$$

with $E_{1/2,\text{irrev}}$ given by Eq. (35).

The plots of the potential versus $\ln(\Psi_{ss} / (\Psi_{ss}^{\text{plateau}} - \Psi_{ss}))$ are linear as can be seen in Fig. 8, allowing the determination of the values of α and k^0 . The applicability of Eq. (46) is restricted in principle to values of $\log(\xi_s) \geq 1.2$. However, this Equation can also be used for smaller values of ξ_s provided the current-potential curve is sigmoidal (i. e. for $\xi_s \geq \xi_{s,\text{lim}}$ which in practice means $\log(\xi_s) \geq 0.32$) with a sufficient potential margin. Thus, we have included in Fig. 8 the transient CV curves obtained for $\log(k_{d,\text{macro}}^0) = -2$ calculated at its $\xi_{s,\text{lim}} (= 1.09)$, along with the corresponding logarithmic plots, from which it can be seen that a good linearity is also obtained in the rising part of the $\Psi - \eta$ curve ($\Psi \leq 0.2$). Thus, under the indicated less restrictive conditions (for $\log(\xi_s) \geq 0.32$), Eqs. (46) can be applied for the analysis of the CV curves in the fully irreversible limit. For example, for values of $D = 10^{-5} \text{ cm}^2 \text{ s}^{-1}$ and $\nu = 0.1 \text{ V s}^{-1}$, Eq. (46) is valid for $r_s \leq 8 \text{ }\mu\text{m}$.

4. Conclusions

An analytical solution has been proposed to characterise the response of a charge transfer process of any degree of reversibility taking place at small spherical or hemispherical electrodes under Cyclic Voltammetry (Eq. (13)). The validity of this solution has been analysed by comparing numerical and analytical curves, thus obtaining accurate results for the transient and stationary response for experimental conditions under which condition $\xi_s (= \sqrt{D/a} / r_s) \geq 1$ holds.

This solution allows a complete characterisation of the current-potential response and a deeper insight of the "macro" and "micro" influences on the irreversibility of the charge transfer process through the definition of a reliable rate constant which is valid for any electrode size and which reflects in a separate way the influences of both factors. This solution also enables us to deduce simpler expressions for both kinetic and geometric limiting behaviors.

From the results obtained, different transitions in the CV curves when moving from macroelectrodes to microelectrodes have been characterized, and the limiting values of parameter ξ_s corresponding to them have been found. Thus, it can be concluded that the CV curve will present a clear peak for values of $\xi_s \leq 1.09$ whatever the degree of reversibility of the charge transfer. For $1.09 \leq \xi_s \leq 15.8$ the CV curves will be sigmoidal in shape although they present a transient character and Eq. (13) should be used for the kinetic analysis (for typical values of $D = 10^{-5} \text{ cm}^2 \text{ s}^{-1}$ and $\nu = 0.1 \text{ V s}^{-1}$, the electrode radius is in the range $(14 \leq r_s \leq 1) \text{ }\mu\text{m}$). Steady-state voltammograms are obtained for $\xi_s > 15.8$ (i. e., $r_s \leq 1 \text{ }\mu\text{m}$ should be used for the values of the diffusion coefficient and scan rate above indicated).

Although the Butler-Volmer model has been used, the treatment followed can be easily extended to a symmetric or asymmetric Marcus-Hush model in the case of extremely small electrodes (electrode radius below $10^{-2} \text{ }\mu\text{m}$) or very low reorganization energies.

It is possible to extend this treatment to other electrode geometries such as bands and discs by simply defining a suitable current normalization and the corresponding expression for the diffusion layer thickness.

5. Acknowledgements

The authors greatly appreciate financial support provided by the Fundación SENECA de la Región de Murcia under the Projects 19887/GERM/15 and 18968/JLI/13, as well as by the Ministerio de Economía y Competitividad under the Projects CTQ2015-71955-REDT (Newtwork of excellence "Sensors and Biosensors") and CTQ2015-65243-P.

REFERENCES

1. A. J. Bard, L. R. Faulkner, *Electrochemical Methods*, 2nd Ed., Wiley, 2001, New York
2. F. Scholz (Ed.), *Electroanalytical Methods: Guide to experiments and applications*, 2nd Ed., Springer, 2010, Weinheim
3. A. Molina, J. Gonzalez, *Pulse Voltammetry in Physical Electrochemistry and Electroanalysis. Theory and Applications*, Springer 2016, Weinheim
4. R. G. Compton, C. E. Banks, *Understanding Voltammetry*, 2nd Ed, Imperial College Press, 2011, London
5. H. H. Girault, *Analytical and Physical Electrochemistry (Fundamental Sciences)*, 1st Ed., EFPL Press, 2004, Lausanne
6. E. Laborda, J. Gonzalez, A. Molina, Recent Advances on the Theory of Pulse Techniques: A mini Review, *Electrochem. Commun.* 43 (2014) 25-30
7. D. Britz, J. Strutwolf, *Digital Simulation in Electrochemistry*, 4th Edition, Springer, 2016, Weinheim
8. R. G. Compton, E. Laborda, K. R. Ward, *Understanding Voltammetry: simulation of electrode processes*, Imperial College Press, 2014, London
9. C. Amatore, O. Klymenko, I. Svir, A new strategy for simulation of electrochemical mechanisms involving acute reaction fronts in solution: Principle, *Electrochem. Commun.* 12 (2010) 1170-1173
10. E. J. F. Dickinson, H. Ekström, E. Fontes, COMSOL Multiphysics®: Finite element software for electrochemical analysis. A mini-review, *Electrochem. Commun.* 40 (2014) 71-74
11. A. Molina, J. Gonzalez, M. Henstringe, R. G. Compton, Voltammetry of Electrochemically Reversible Systems at Electrodes of any Geometry: A General, Explicit Analytical Characterisation, *J. Phys. Chem. C* 115 (2011) 4054-4062
12. L. K. Bieniasz, A new theory, and automatic computation of reversible cyclic voltammograms at a microband electrode, *J. Electroanal. Chem.* 767 (2016) 123-133
13. K. B. Oldham, J. C. Myland, Modelling cyclic voltammetry without digital simulation, *Electrochim. Acta* 56 (2011) 10612-10625
14. P. J. Mahon, K. B. Oldham, Convolutional modelling of the disk electrode geometry under reversible conditions, *Electrochim. Acta* 49 (2004) 5049-5054
15. Parveen, R. Kant, Theory for staircase voltammetry and linear scan voltammetry on fractal electrodes: Emergence of anomalous Randles–Ševčík behavior, *Electrochim. Acta* 111 (2013) 223-233
16. K. B. Oldham, Steady-state voltammetry at microelectrodes of arbitrary shape, *J. Electroanal. Chem.* 323 (1992) 53-76
17. A. Molina, J. Gonzalez, E. Laborda, R. G. Compton, Analytical solutions for fast and straightforward study of the effect of the electrode geometry in transient and steady state

voltammetries: Single- and multi-electron transfers, coupled chemical reactions and electrode kinetics, *J. Electroanal. Chem.* 756 (2015) 1-21

18. J. Kim, A. J. Bard, Application of the Koutecký-Levich Method to the Analysis of Steady State Voltammograms with Ultramicroelectrodes, *Anal. Chem.*, 88 (2016) 1742-1747

19. K. Aoki, Evaluation technique of kinetic parameters for irreversible charge transfer reactions from steady-state voltammograms at microdisk electrodes, *Electrochem. Commun.* 7 (2005) 523-527

20. K. J. Aoki, Voltammetry at a single nano-electrode by varying electrode diameters: Review, *J. Electroanal. Chem.*, in press, doi: [dx.doi.org/10.1016/j.jelechem.2016.03.029](https://doi.org/10.1016/j.jelechem.2016.03.029)

21. A. Molina, J. Gonzalez, E. O. Barnes, R. G. Compton, Simple analytical equations for the current-potential curves at microelectrodes: A universal approach *J Phys Chem C* 118 (2014) 346-356

22. K. B. Oldham, J. C. Myland, A. M. Bond, *Electrochemical science and technology: fundamentals and applications*, Wiley, 2011

23. A. M. Bond, E. A. Mashkina, A. N. Simonov, A critical review of methods available for quantitative evaluation of electrode kinetics at stationary macrodisk electrodes, in D. Pletcher, Z-Q. Tian, D. E. Williams (Eds) *Developments in Electrochemistry. Science inspired by Martin Fleischmann*, Wiley, 2014, Chichester

24. M. C. Henstridge, E. Laborda, N. Rees, R. G. Compton, Marcus–Hush–Chidsey theory of electron transfer applied to voltammetry: A review, *Electrochim. Acta*, 84 (2012) 12-20

25. A. Molina, C. Serna, L. Camacho, Conditions of applicability of the superposition principle in potential multipulse techniques: implications in the study of microelectrodes, *J. Electroanal Chem* 394 (1995) 1-6

26. S. Fletcher, The theory of electron transfer, *J. Solid Stat. Electrochem.* 14 (2010) 705-739

27. M. C. Henstridge, E. Laborda, E. J. F. Dickinson, R. G. Compton, Redox systems obeying Marcus–Hush–Chidsey electrode kinetics do not obey the Randles–Ševčík equation for linear sweep voltammetry, *J. Electroanal. Chem.*, 664 (2012) 73-99

28. W-J. Lan, H. S. White, S. Chen, Electrical double-layer effects on electron transfer and ion transfer at the nanoscale in M. V. Mirking, S. Amemiya (Eds.), *Nanoelectrochemistry*, CRC Press, 2015, Boca Raton

29. R. Guidelli, R. G. Compton, J. M. Feliu, E. Guileadi, J. Lipkowski, W. Schmickler, S. Trasatti, Defining the transfer coefficient in electrochemistry: An assessment (IUPAC Technical Report), *Pure Appl. Chem.* 86 (2014) 245-258

30. R. Guidelli, R. G. Compton, J. M. Feliu, E. Gileadi, J. Lipkowski, W. Schmickler, S. Trasatti, Definition of the transfer coefficient in electrochemistry (IUPAC Recommendations 2014), *Pure Appl. Chem.* 86 (2014) 259-262

31. K. B. Oldham, J. C. Myland General theory of steady-state voltammetry, *J. Electroanal Chem* 347 (1993) 49-91
32. E. J. Calvo, A. J. Bard, M. Stratmann (Eds), *Encyclopedia of Electrochemistry Vol. 2*, Wiley-VCH, Weinheim, 2003
33. A. Molina, J. Gonzalez, F. Martinez-Ortiz, R. G. Compton, Geometrical insights of transient diffusion layers, *J. Phys Chem C* 114 (2010) 4093-4099
34. A. Molina, E. Laborda, J. Gonzalez, R. G. Compton, On the Meaning of the Diffusion Layer Thickness for Slow Electrode Reactions, *Phys Chem Chem Phys.* 15 (2013) 2381-2388
35. A. Molina, E. Laborda, J. Gonzalez, R. G. Compton, Effects of convergent diffusion and charge transfer kinetics on the diffusion layer thickness of spherical micro- and nanoelectrodes, *Phys Chem Chem Phys.* 15 (2013) 7106-7113
36. H. Matsuda, Y. Ayabe, Zur Theorie der Randles-Sevčikschen Kathodenstrahl-Polarographie, *Zeitschrift für Elektrochemie Z. Elektrochem* 59 (1955) 494-503
37. A. Molina, J. Gonzalez, E. Laborda, F. Martinez-Ortiz, L. K. Bieniasz, Electrocatalysis at modified microelectrodes. A theoretical approach to cyclic voltammetry, *J. Phys. Chem. C* 114 (2010)14552-14551
38. K. B. Oldham, J. Myland, J. Spanier, *An atlas of functions*, 2nd Ed., Springer, 2009, New York
39. A. Molina, C. Serna, F. Martinez-Ortiz, E. Laborda, Potentiostatic voltammetry at spherical electrodes and microelectrodes in the presence of product, *J. Electroanal. Chem.* 617(2008)14-26
40. F. Martinez-Ortiz, A. Molina, E. Laborda, Electrochemical digital simulation with high expanding four point discretization: Can Crank-Nicolson uncouple diffusion and homogenous chemical reactions?, *Electrochim. Acta* 56 (2011)5707-5716
41. F. Martinez-Ortiz, N. Zorua, E. Laborda, A. Molina, Brute force (or not so brute) digital simulation in electrochemistry revisited, *Chem. Phys. Lett.* 643(2016)71-76

Equation Chapter 1 Section 1 Appendix A.

A.1. Application of a potential pulse, E_1

The mass transport of species O and R in electrode reaction (I) when applying a potential pulse, E_1 , to a spherical or hemispherical electrode of radius r_s during a time $0 \leq t \leq \tau$, is described by the following diffusive differential equation system:

$$\hat{O}c_O^1(r,t) = \hat{O}c_R^1(r,t) = 0 \quad (A1)$$

where

$$\hat{O} = \frac{\partial}{\partial t} - D \left(\frac{\partial^2}{\partial r^2} + \frac{2}{r} \frac{\partial}{\partial r} \right) \quad (A2)$$

$c_O^1(r,t)$ and $c_R^1(r,t)$ are the concentration profiles of species O and R and D is the diffusion coefficient of both species assumed as equal. In this section, superscript "1" refers to the first potential pulse applied, E_1 .

The boundary value problem when only species O is initially present is given by

$$\left. \begin{array}{l} t \geq 0, r \rightarrow \infty \\ t = 0, r \geq r_s \end{array} \right\} \quad c_O^1(r,t) = c_O^*, \quad c_R^1(r,t) = 0 \quad (A3)$$

$$t > 0, r = r_s,$$

$$\left(\frac{\partial c_O^1}{\partial r} \right)_{r=r_s} = - \left(\frac{\partial c_R^1}{\partial r} \right)_{r=r_s} \quad (A4)$$

$$\frac{I^1}{FA_s} = D \left(\frac{\partial c_O^1}{\partial r} \right)_{r=r_s} = k_{\text{red}}^1 c_O^{(s,1)} - k_{\text{ox}}^1 c_R^{(s,1)} \quad (A5)$$

$c_O^{(s,1)}$ and $c_R^{(s,1)}$ are the surface concentrations of species O and R which, in general, are time and potential dependent. I^1 is the current obtained, F the Faraday constant and A_s the area of the electrode.

From Eq. (A4), it can be noted that the total concentration of the electroactive species remains constant in time and distance to the electrode whatever the degree of reversibility of the charge transfer process. Thus, under the above conditions, the following is hold [11, 17]:

$$c_O^1(r,t) + c_R^1(r,t) = c_O^* \quad (A6)$$

Thus, this problem can be reduced to the finding of a single unknown concentration ($c_O^1(r,t)$) and Eqs. (A1)-(A5) become

$$\hat{O}c_O^1(r,t) = 0 \quad (A7)$$

$$\left. \begin{array}{l} t \geq 0, r \rightarrow \infty \\ t = 0, r \geq r_s \end{array} \right\} \quad c_O^1(r,t) = c_O^* \quad (A8)$$

$t > 0, r = r_s,$

$$\frac{I^1}{FA_s} = D \left(\frac{\partial c_O^1}{\partial r} \right)_{r=r_s} = (k_{\text{red}}^1 + k_{\text{ox}}^1) c_O^{(s,1)} - k_{\text{ox}}^1 c_O^* \quad (\text{A9})$$

By following a similar procedure to that in references [11, 17, 37], it will be assumed that the concentration profile of species O can be written in an approximate way as that for a nernstian process,

$$c_O^1(r, t) = c_O^* + \frac{r_s}{r} \left(c_O^{(s,1)} - c_O^* \right) \text{erfc} \left(\frac{r - r_s}{2\sqrt{Dt}} \right) \quad (\text{A10})$$

with $\text{erfc}(x)$ being the complementary error function [38]. Thus, the surface gradient of species O can be written as

$$\left(\frac{\partial c_O^1}{\partial r} \right)_{r=r_s} = \frac{c_O^* - c_O^{(s,1)}}{\delta_s^1(r_s, t)} \quad (\text{A11})$$

where

$$\delta_s^1(r_s, t) = \frac{1}{\frac{1}{\sqrt{\pi Dt}} + \frac{1}{r_s}} \quad (\text{A12})$$

$\delta_s^1(r_s, t)$ is the diffusion layer thickness corresponding to a fast electrode charge process taking place at a spherical or hemispherical electrode of radius r_s [3, 33].

By inserting Eq. (A11) into Eq. (A9) the following expression for the surface concentration of oxidised species, $c_O^{(s,1)}$, is obtained

$$\frac{c_O^{(s,1)}}{c_O^*} = \frac{1 + k_T^{0,1}}{1 + k_T^{1,1}} + \frac{k_{\text{ox}}^{1,1} - k_{\text{ox}}^{0,1}}{1 + k_T^{1,1}} \quad (\text{A13})$$

with

$$k_T^{1,1} = \frac{(k_{\text{red}}^1 + k_{\text{ox}}^1) \delta_s^1(r_s, t)}{D} \quad (\text{A14})$$

$$k_{\text{ox}}^{1,1} = \frac{k_{\text{ox}}^1 \delta_s^1(r_s, t)}{D} \quad (\text{A15})$$

and $k_T^{0,1} = k_{\text{ox}}^{0,1} = 0$.

By incorporating Eqs. (A13)-(A15) into Eq. (A9) the following expression for the current is obtained:

$$\frac{I^1}{I_d^1} = k_T^{1,1} \left(\frac{c_O^{(s,1)}}{c_O^*} \right) - k_{\text{ox}}^{1,1} = k_T^{1,1} \left(\frac{1 + k_T^{0,1}}{1 + k_T^{1,1}} + \frac{k_{\text{ox}}^{1,1} - k_{\text{ox}}^{0,1}}{1 + k_T^{1,1}} \right) - k_{\text{ox}}^{1,1} \quad (\text{A16})$$

and

$$I_d^1 = FA_s D c_O^* \frac{1}{\delta_s^1(r_s, t)} \quad (A17)$$

with I_d^1 being the diffusion limiting current for a spherical or hemispherical electrode [1, 3, 33].

A.2. Application of a second potential pulse, E_2

If for a time $t > \tau$ a second potential pulse, E_2 , is applied during a time $0 \leq t_2 \leq \tau$ (with $t = \tau + t_2$), and taking into account that the concentration profiles of species O and R fulfil

$$c_O^2(r, t) + c_R^2(r, t) = c_O^* \quad (A18)$$

the mass transport problem can be written as

$$\hat{O}_2 c_O^2(r, t) = 0 \quad (A19)$$

with

$$\hat{O}_2 = \frac{\partial}{\partial t_2} - D \left(\frac{\partial^2}{\partial r^2} + \frac{2}{r} \frac{\partial}{\partial r} \right) \quad (A20)$$

$$\left. \begin{array}{l} t_2 \geq 0, r \rightarrow \infty \\ t_2 = 0, r \geq r_s \end{array} \right\} \quad c_O^2(r, t) = c_O^1(r, t) \quad (A21)$$

$$t_2 > 0, r = r_s,$$

$$\frac{I^2}{FA_s} = D \left(\frac{\partial c_O^2}{\partial r} \right)_{r=r_s} = (k_{\text{red}}^2 + k_{\text{ox}}^2) c_O^{(s,2)} - k_{\text{ox}}^2 c_O^* \quad (A22)$$

$c_O^1(r, t)$ is given by Eq. (A10) for $t = \tau + t_2$. Superscript "2" refers in this section to the second potential pulse applied, E_2 .

It will be assumed, in an analogous way to that for the first pulse, E_1 , that the expression for the concentration profile of species O can be written as [11]

$$c_O^2(r, t) = c_O^* + \frac{r_s}{r} \left[\left(c_O^{(s,1)} - c_O^* \right) \text{erfc} \left(\frac{r - r_s}{2\sqrt{D(\tau + t_2)}} \right) + \left(c_O^{(s,2)} - c_O^{(s,1)} \right) \text{erfc} \left(\frac{r - r_s}{2\sqrt{Dt_2}} \right) \right] \quad (A23)$$

and the surface gradient of species O is given by

$$\left(\frac{\partial c_O^2}{\partial r} \right)_{r=r_s} = \frac{c_O^* - c_O^{(s,1)}}{\delta_s^1(r_s, \tau + t_2)} + \frac{c_O^{(s,1)} - c_O^{(s,2)}}{\delta_s^2(r_s, t_2)} \quad (A24)$$

where

$$\delta_s^2(r_s, t_2) = \frac{1}{\frac{1}{\sqrt{\pi D t_2}} + \frac{1}{r_s}} \quad (A25)$$

By inserting Eq. (A24) into Eq. (A22) the following expression for the surface concentration of oxidised species, $c_O^{(s,2)}$, is obtained

$$\begin{aligned}\frac{c_O^{(s,2)}}{c_O^*} &= \left(\frac{c_O^{(s,1)}}{c_O^*} \right) \frac{1+k_T^{1,2}}{1+k_T^{2,2}} + \frac{k_{ox}^{2,2} - k_{ox}^{1,2}}{1+k_T^{2,2}} = \\ &= \frac{1+k_T^{0,1}}{1+k_T^{1,1}} \frac{1+k_T^{1,2}}{1+k_T^{2,2}} + \frac{k_{ox}^{1,1} - k_{ox}^{0,1}}{1+k_T^{1,1}} \frac{1+k_T^{1,2}}{1+k_T^{2,2}} + \frac{k_{ox}^{2,2} - k_{ox}^{1,2}}{1+k_T^{2,2}}\end{aligned}\quad (A26)$$

with

$$k_T^{h,2} = \frac{(k_{red}^i + k_{ox}^i) \delta_s^2(r_s, t_2)}{D} \quad h=1, 2 \quad (A27)$$

$$k_{ox}^{h,2} = \frac{k_{ox}^i \delta_s^2(r_s, t_2)}{D} \quad h=1, 2 \quad (A28)$$

The current corresponding to this second pulse can be obtained by inserting Eqs. (A26)-(A28) in Eq. (A22),

$$\begin{aligned}\frac{I^2}{FA_s D c_O^* \frac{1}{\delta_s^2(r_s, t_2)}} &= k_T^{2,2} \left(\frac{c_O^{(s,2)}}{c_O^*} \right) - k_{ox}^{2,2} = \\ &= k_T^{2,2} \left(\frac{1+k_T^{1,2}}{(1+k_T^{1,1})(1+k_T^{2,2})} + \frac{k_{ox}^{1,1} - k_{ox}^{0,1}}{1+k_T^{1,1}} \frac{1+k_T^{1,2}}{1+k_T^{2,2}} + \frac{k_{ox}^{2,2} - k_{ox}^{1,2}}{1+k_T^{2,2}} \right) - k_{ox}^{2,2}\end{aligned}\quad (A29)$$

A.3. Application of a sequence of potential pulses, $E_1, E_2, \dots, E_j, \dots, E_p$

We will consider now that a j -th potential pulse E_j is applied during a time $0 \leq t_j \leq \tau$, with the total time being

$$t = (j-1)\tau + t_j \quad (A30)$$

Taking into account that the concentration profiles of species O and R fulfil

$$c_O^j(r, t) + c_R^j(r, t) = c_O^* \quad (A31)$$

the boundary value problem for the j -th potential pulse can be written in the following general way:

$$\hat{O}_j c_O^j(r, t) = 0 \quad (A32)$$

with

$$\hat{O}_j = \frac{\partial}{\partial t_j} - D \left(\frac{\partial^2}{\partial r^2} + \frac{2}{r} \frac{\partial}{\partial r} \right) \quad (A33)$$

$$\left. \begin{aligned} t_j &\geq 0, \quad r \rightarrow \infty \\ t_j &= 0, \quad r \geq r_s \end{aligned} \right\} \quad c_O^j(r, t) = c_O^{j-1}(r, t) \quad (A34)$$

$$t_j > 0, r = r_s, \quad \frac{I^j}{FA_s} = D \left(\frac{\partial c_O^j}{\partial r} \right)_{r=r_s} = (k_{\text{red}}^j + k_{\text{ox}}^j) c_O^{(s,j)} - k_{\text{ox}}^j c_O^* \quad (\text{A35})$$

where superscript "j" refers to the j-th potential pulse applied and $c_O^0(r, t) = c_O^*$.

The concentration profile of species O, $c_O^j(r, t)$, can be written as a function of those obtained in previous potential pulses in the following approximate way [11]:

$$c_O^j(r, t) = c_O^* + \frac{r_s}{r} \sum_{l=1}^j \left[\left(c_O^{(s,l)} - c_O^{(s,l-1)} \right) \text{erfc} \left(\frac{r - r_s}{2\sqrt{Dt_{l,j}}} \right) \right] \quad (\text{A36})$$

with $c_O^{(s,0)} = c_O^*$ and

$$\left. \begin{aligned} t_{l,j} &= (j-l)\tau + t_j \\ t_{j,j} &\equiv t_j \end{aligned} \right\} \quad (\text{A37})$$

Thus, the surface gradient of species O is given by

$$\left(\frac{\partial c_O^j}{\partial r} \right)_{r=r_s} = \sum_{l=1}^j \left[\frac{c_O^{(s,l-1)} - c_O^{(s,l)}}{\delta_s^l(r_s, t_{l,j})} \right] \quad (\text{A38})$$

where

$$\delta_s^l(r_s, t_{l,j}) = \frac{1}{\frac{1}{\sqrt{\pi D t_{l,j}}} + \frac{1}{r_s}} \quad (\text{A39})$$

By operating in the same way as indicated for the second potential pulse applied, the following expression for the surface concentration of species O, $c_O^{(s,j)}$, is found:

$$\frac{c_O^{(s,j)}}{c_O^*} = \frac{\prod_{l=1}^j (1 + k_T^{l-1,l})}{\prod_{l=1}^j (1 + k_T^{l,l})} + \sum_{l=1}^j \left(k_{\text{ox}}^{l,l} - k_{\text{ox}}^{l-1,l} \right) \frac{\prod_{m=l}^{j-1} (1 + k_T^{m,m+1})}{\prod_{m=l}^j (1 + k_T^{m,m})} \quad (\text{A40})$$

where

$$k_T^{h,i} = \frac{(k_{\text{red}}^h + k_{\text{ox}}^h) \delta_s^i(r_s, t_{i,j})}{D} \quad h, i=1, 2, \dots, j \quad (\text{A41})$$

$$k_{\text{ox}}^{h,i} = \frac{k_{\text{ox}}^h \delta_s^i(r_s, t_{i,j})}{D} \quad h, i=1, 2, \dots, j \quad (\text{A42})$$

By inserting Eqs. (A40)-(A42) into (A35) the following expression for the current is obtained

$$\begin{aligned}
\frac{I^j}{FA_s D c_O^* \frac{1}{\delta_s^j(r_s, t_j)}} &= k_T^{j,j} \left(\frac{c_O^{(s,j)}}{c_O^*} \right) - k_{ox}^{j,j} = \\
&= k_T^{j,j} \left(\frac{\prod_{l=1}^j (1 + k_T^{l-1,l})}{\prod_{l=1}^j (1 + k_T^{l,l})} + \sum_{l=1}^j \left(k_{ox}^{l,l} - k_{ox}^{l-1,l} \right) \frac{\prod_{m=l}^{j-1} (1 + k_T^{m,m+1})}{\prod_{m=l}^j (1 + k_T^{m,m})} \right) - k_{ox}^{j,j}
\end{aligned} \tag{A43}$$

This expression can be applied to any multipotential pulse technique such as Differential Double Pulse Voltammetry, Staircase Voltammetry or Square Wave Voltammetry [3].

Appendix B.

The approximate solution proposed for the dimensionless current (Eq. (13)) has been tested by comparison with results obtained from numerical calculations carried out by applying a finite differences method in the way discussed in references [39-41].

Figure B1 shows the influence of the electrode kinetics, through parameter $k_{d,macro}^0$ (Eq. (20)), shown in the Figures, on the dimensionless CV response ($\psi - \eta$ curves for which the superscript "j" has been removed for simplicity), calculated for two values of ξ_s (Eq. (11)): 1 and 0.1 (on the curves). Solid and dashed lines correspond to analytical (Eq. (13)) and numerical calculations, respectively.

< Figure B1 >

From this Figure it can be seen that for $\xi_s = 1$, whatever the degree of reversibility of the charge transfer, there is a good agreement between the CV curves calculated from Eq. (13) and those obtained numerically (with a maximum error corresponding to the peak current or peak plateau of 1%, see Fig. B2c). In the case of $\xi_s = 0.1$, greater differences are observed in the peak current as the process becomes more irreversible (with errors of around 15% in the peak heights of the CV response for fully irreversible processes, see Fig. B2c).

Figure B2 shows the differences between the analytical and numerical results for peak potentials (B2a), half-peak potentials (B2b) and the relative error in the peak currents (B2c), versus $\log(k_{d,macro}^0)$, for several values of $\log(\xi_s)$ (shown on the curves). From results in Fig. B2c, a zone diagram has been plotted (Fig. B2d) to define the values of $\log(k_{d,macro}^0)$ and $\log(\xi_s)$ which enables us to apply the solution proposed in Eq. (13) with errors below 5% in the measurement of the peak current or peak plateau.

< Figure B2 >

In Fig. B2a it can be seen that the differences in the peak potentials are minor or equal to 5 mV in the macroelectrode limit (see curves with $\log(\xi_s) = -1.5$ and -2) for any degree of reversibility and therefore, although Eq. (13) yields to important errors in the peak currents under these conditions, it can be used in order to calculate accurate values of the peak potentials. The differences increase up to 8-18 mV for intermediate electrode sizes when the process behaves as fully irreversible (see curves with $\log(\xi_s)$ in the range $(-1, 0)$).

Otherwise, the values of half-peak potentials (or half-wave potentials) shows a much better agreement between analytical and numerical results, and the differences observed are below 5 mV for $\log(\xi_s) < -1$ (see Fig. B2b), whatever the degree of reversibility.

From Figs. B2c and B2d it can be seen that for small electrodes ($\log(\xi_s) > -0.4$), the errors in the peak or plateau currents are below 5% whatever the reversibility of the process. Moreover, for $\log(k_{d,\text{macro}}^0) > 0.7$ the errors are below 5% whatever the electrode size. Consequently, the higher errors correspond to macroelectrodes for fully irreversible processes ($\log(\xi_s) < -0.4, \log(k_{d,\text{macro}}^0) < 0.7$). Therefore, the considerations made for the peak current on the basis of Eq. (13) for non-reversible processes and $\log(\xi_s) < -0.4$, should be considered as estimations.

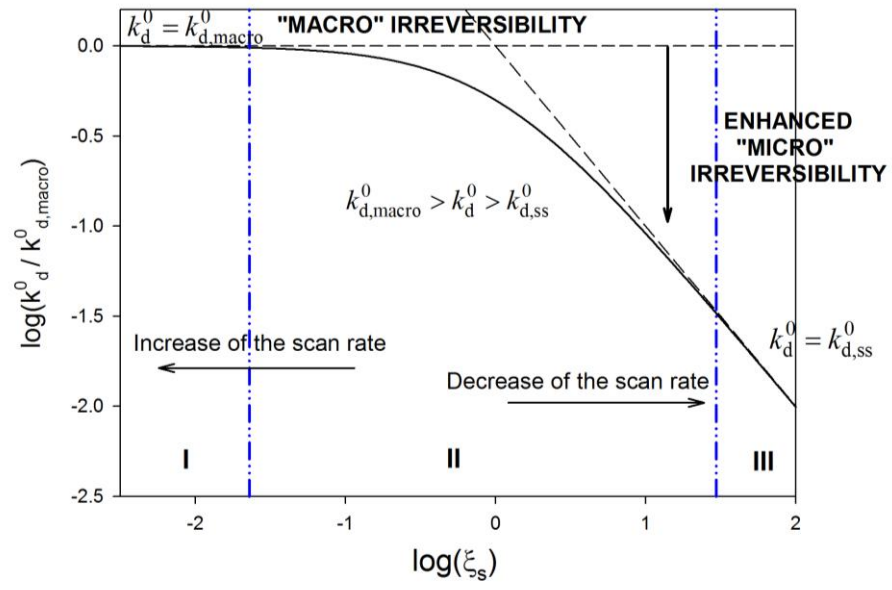


Figure 1

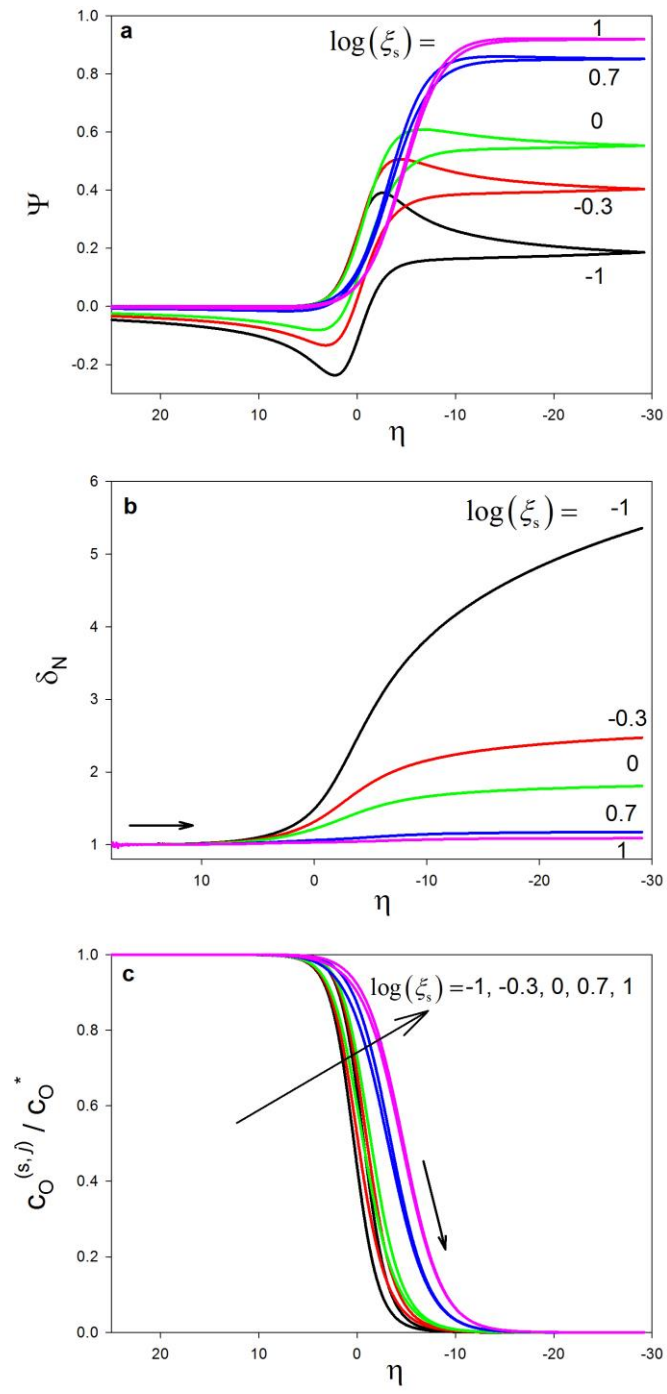


Figure 2

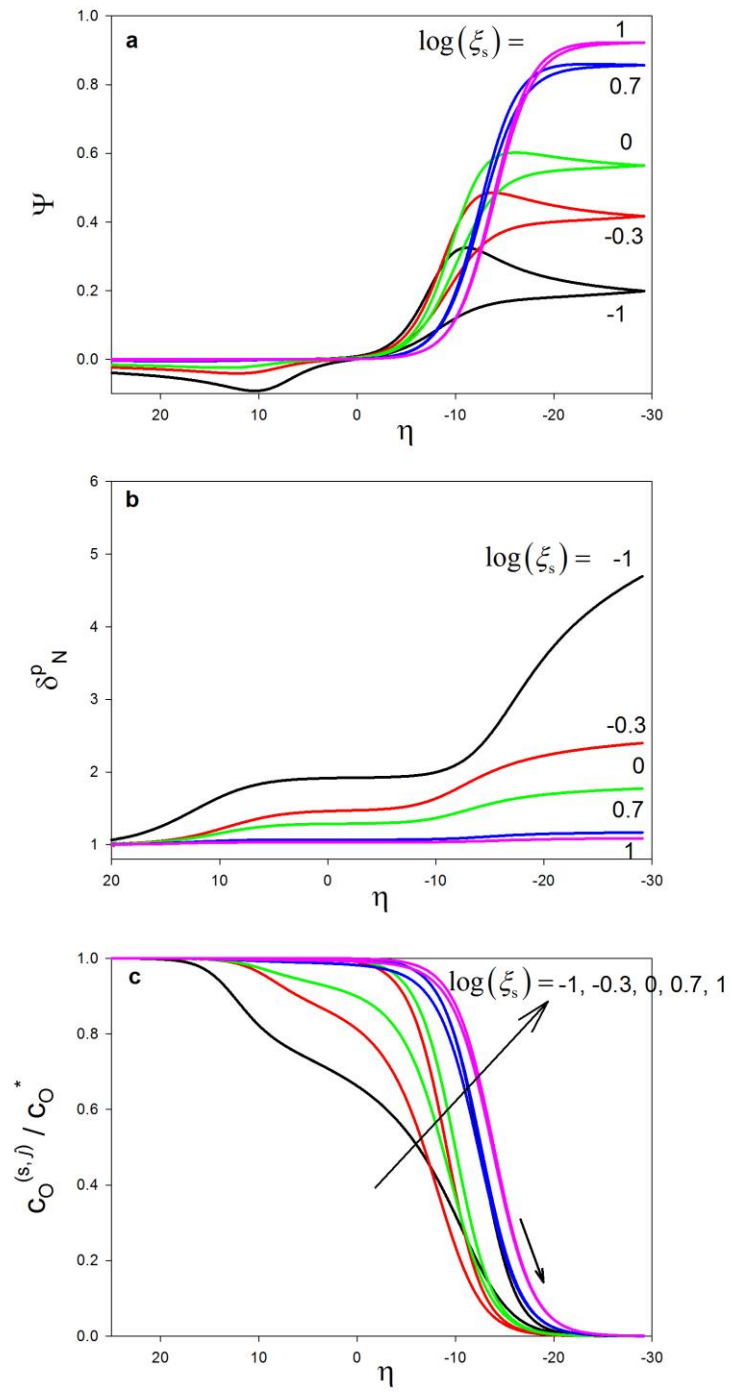


Figure 3

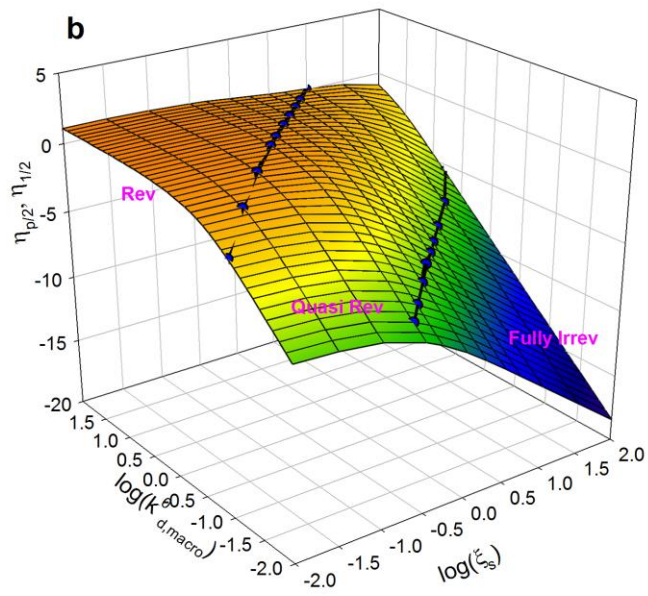
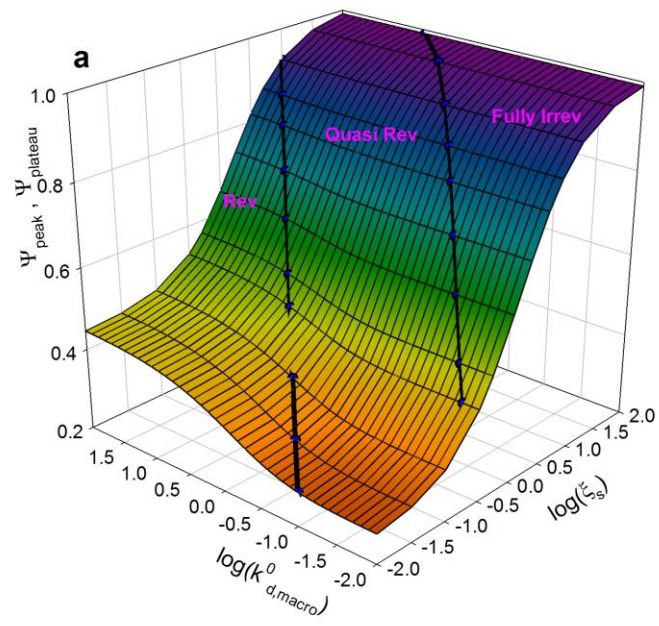


Figure 4

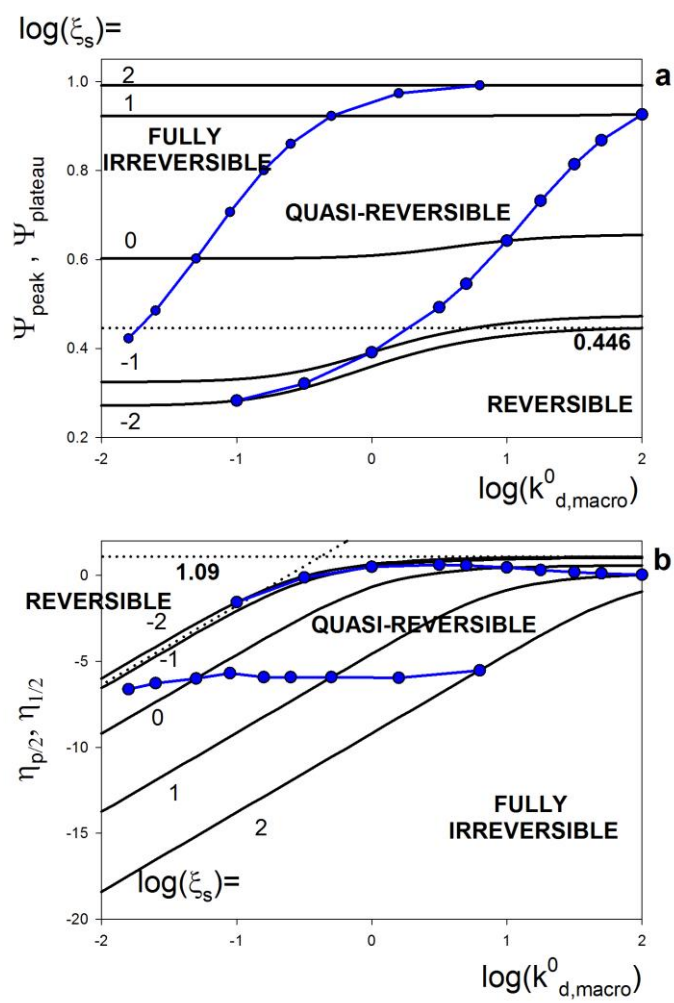


Figure 5

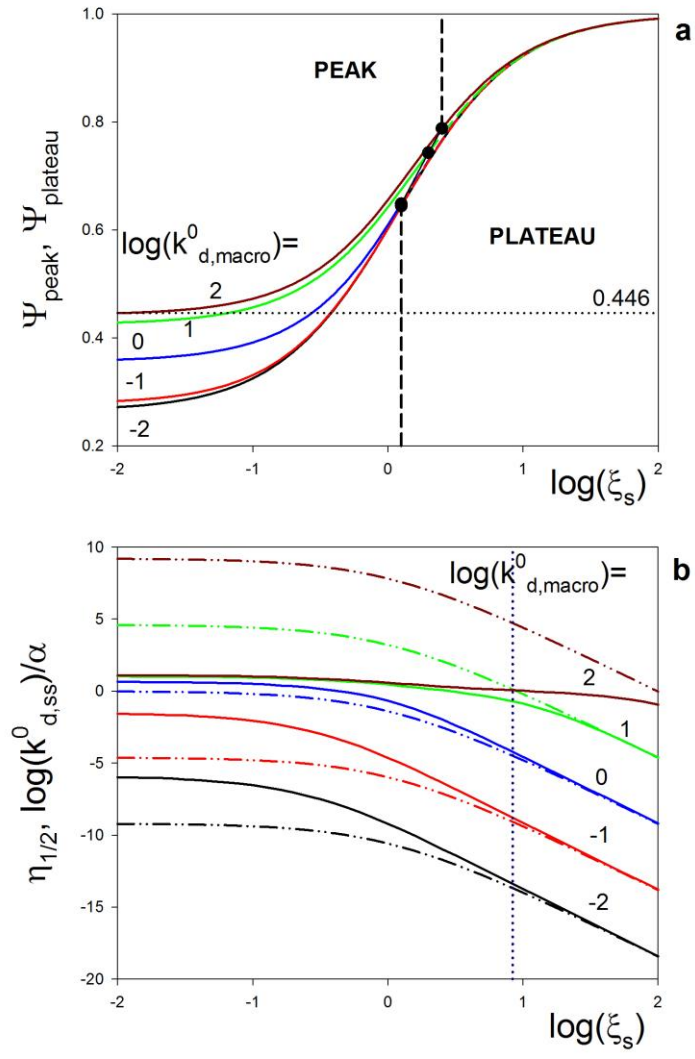


Figure 6

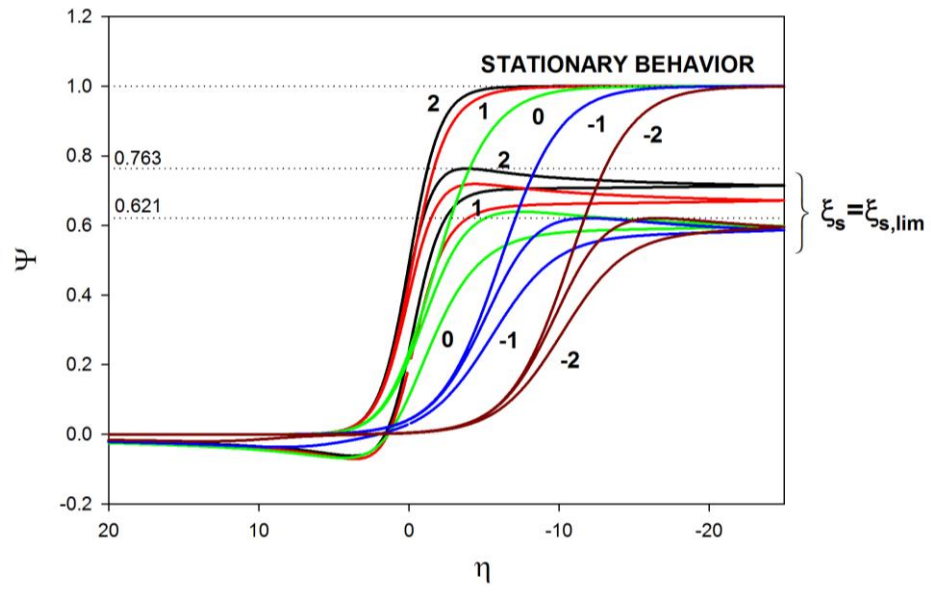


Figure 7

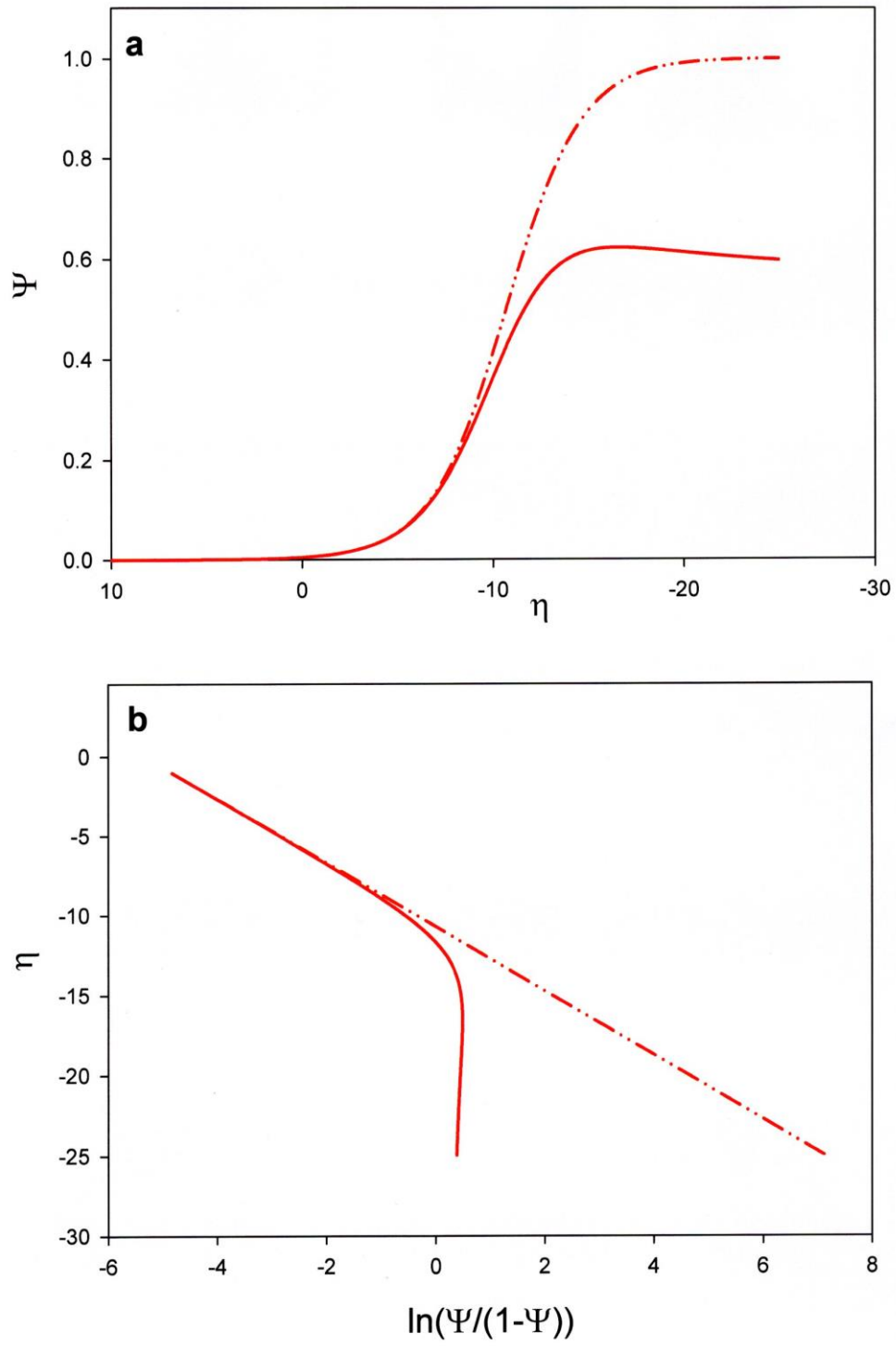


Figure 8

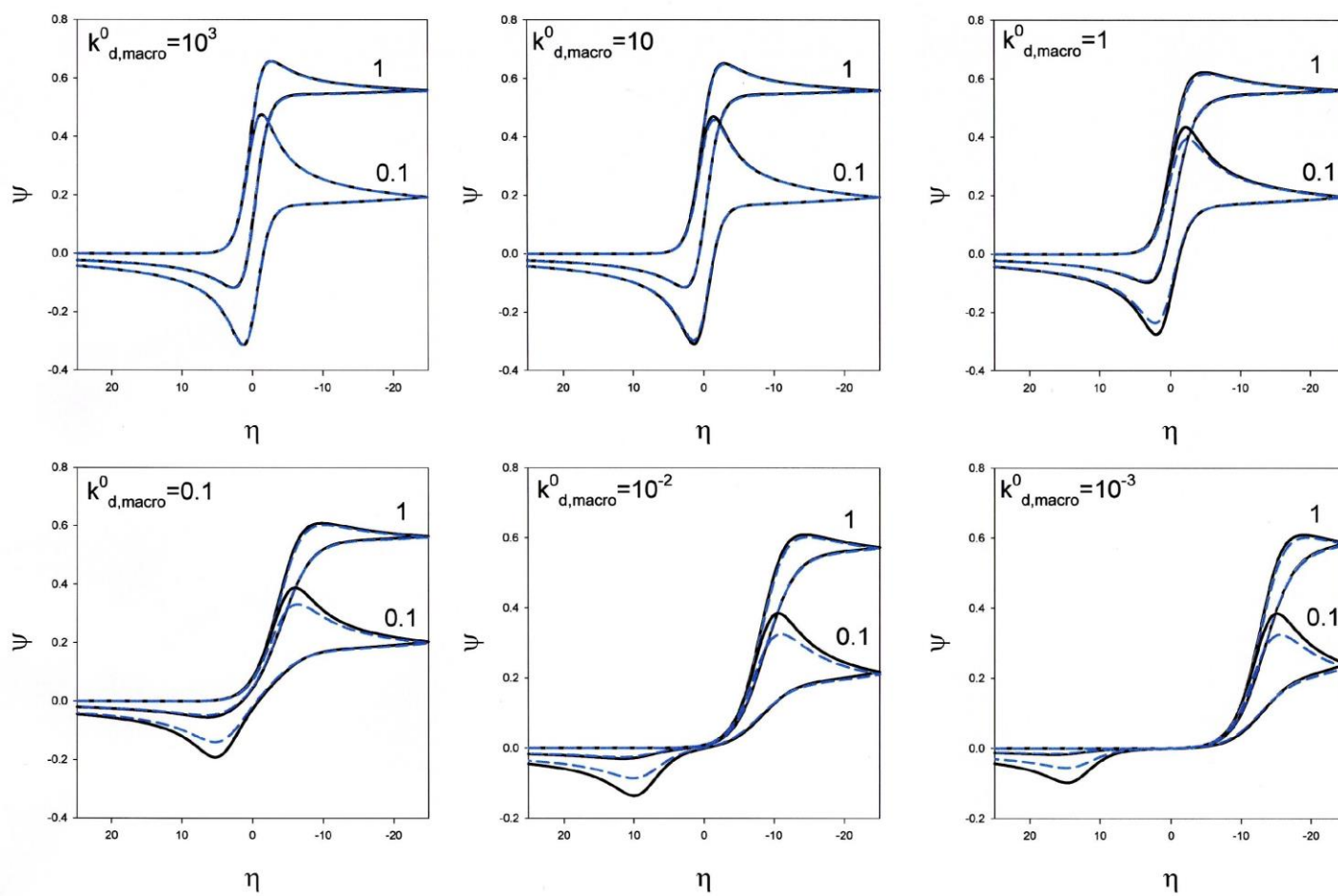


Figure B1

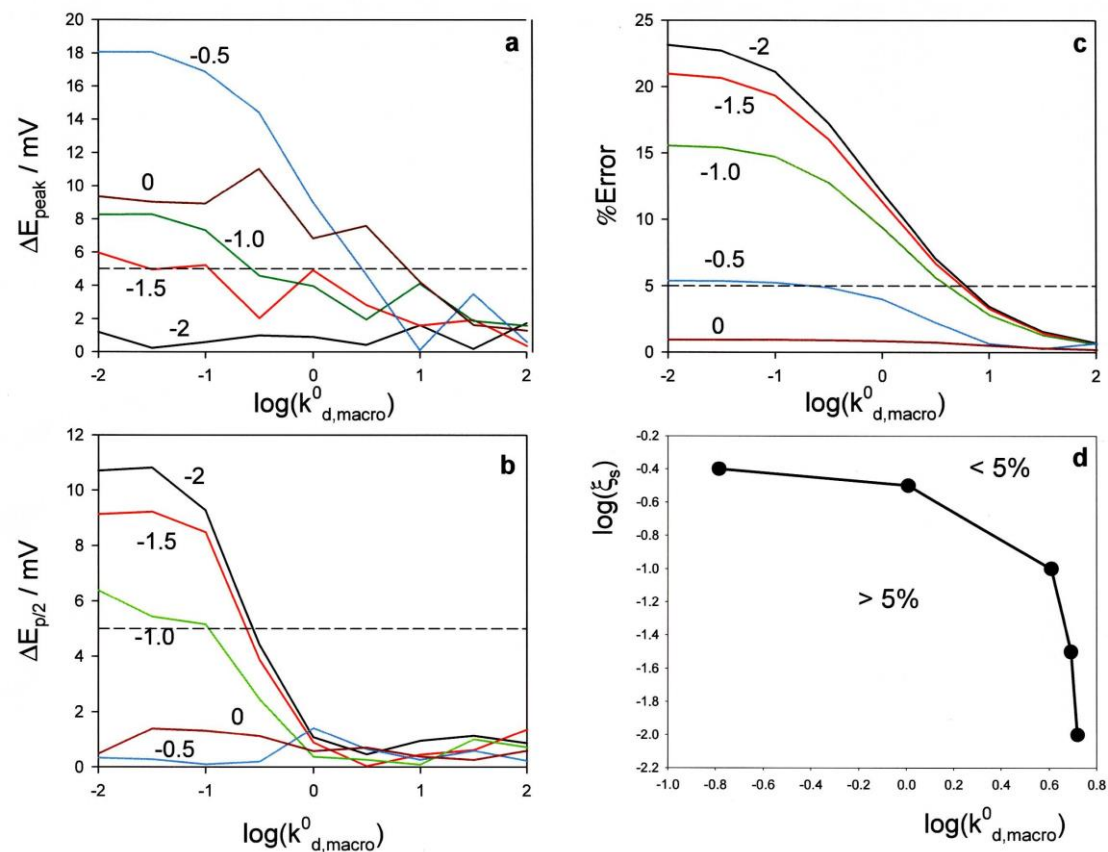
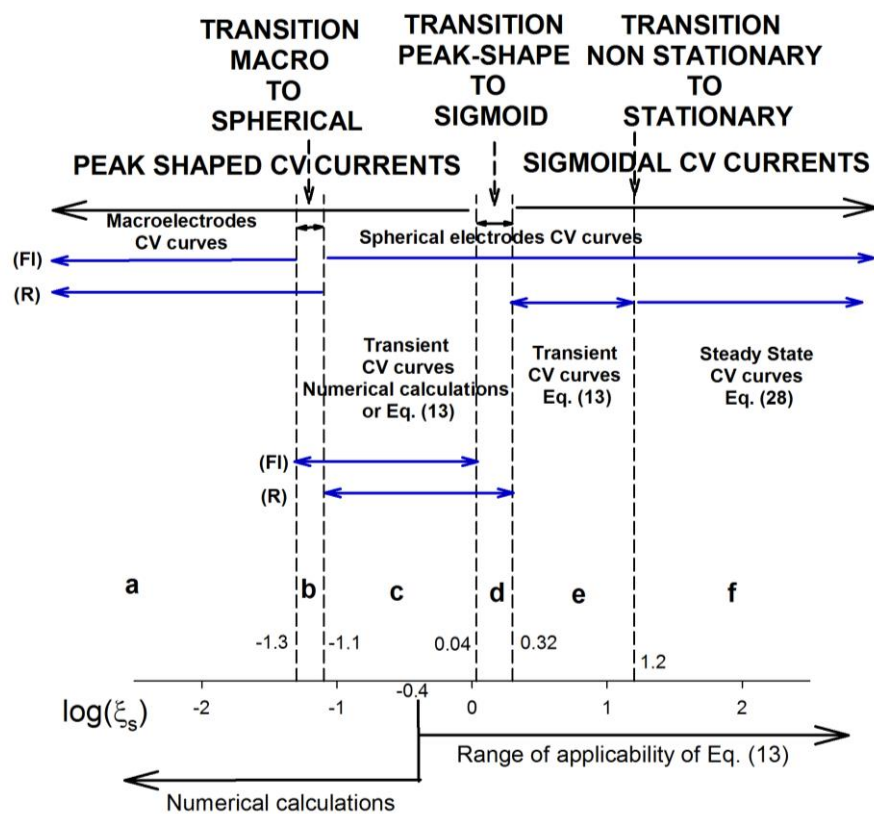
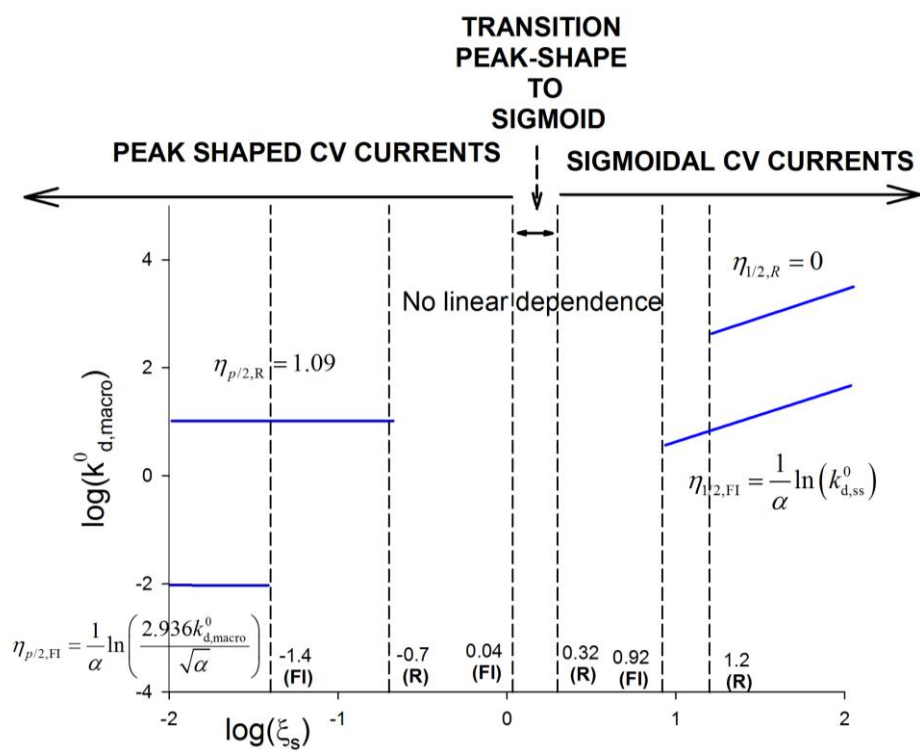


Figure B2



Scheme I



Scheme II

FIGURE LEGENDS

Figure 1. Variation of $\log(k_d^0 / k_{d,macro}^0)$ with $\log(\xi_s)$ calculated from Eqs. (7) and (20).

Limiting values corresponding to $k_{d,macro}^0$ and $k_{d,ss}^0 = (k_{d,macro}^0 / \xi_s)$ are also shown in the Figure.

Figure 2. Influence of ξ_s on the $\Psi - \eta$ curves (a, Eq. (13)), on the dimensionless diffusion layer thickness $\delta_N = \delta_{CV} / (1 + \xi_s) \sqrt{D/a}$ (b, see Eq. (36)), and on the surface concentrations (c, Eq. (3)). The values of ξ_s appear on the curves. $k_{d,macro}^0 = 1$, $\alpha = 0.5$. The values of δ_N correspond to the direct scan.

Figure 3. Influence of ξ_s on the $\Psi - \eta$ curves (a, Eq. (13)), on the dimensionless diffusion layer thickness $\delta_N = \delta_{CV} / (1 + \xi_s) \sqrt{D/a}$ (b, see Eq. (36)), and on the surface concentrations (c, Eq. (3)). The values of ξ_s appear on the curves. $k_{d,macro}^0 = 10^{-2}$, $\alpha = 0.5$. The values of δ_N correspond to the direct scan.

Figure 4. Variation of the dimensionless peak current $\Psi_{peak} / \Psi_{plateau}$ (a), and the half-peak $\eta_{p/2} / \eta_{1/2}$ (b) of the CV curves with the electrode kinetics (through $\log(k_{d,macro}^0)$) and with the electrode size (through $\log(\xi_s)$). Lines with symbols mark the limit values of k_d^0 corresponding to reversible, quasi-reversible and fully irreversible behavior (see Eq. (42)). $\alpha = 0.5$.

Figure 5. Variation of the dimensionless peak current $\Psi_{peak} / \Psi_{plateau}$ (a), and half-peak $\eta_{p/2} / \eta_{1/2}$ (b) of the CV curves of spherical electrodes with $\log(k_{d,macro}^0)$ calculated for several values of $\log(\xi_s)$ shown in the curves. Blue lines with symbols in Figs a and b mark the limit values of k_d^0 corresponding to reversible, quasi-reversible and fully irreversible behavior (see Eqs. (7) and (42)). $\alpha = 0.5$.

Figure 6. Variation of the dimensionless peak current $\Psi_{peak} / \Psi_{plateau}$ (a), and half-peak $\eta_{p/2} / \eta_{1/2}$ (b) of the Cyclic Voltammetry curves of spherical electrodes with $\log(\xi_s)$ calculated for several values of $\log(k_{d,macro}^0)$ shown in the curves. Black dots in Fig. a correspond to the limit values of $\log(\xi_s)$ for which the peak current does

not differ more than a 5% of the limiting current (see discussion). The variation of $\log(k_{d,ss}^0)/\alpha \log(\xi_s)$ calculated from Eq. (35) has been included in Fig. b (dashed-dotted lines). $\alpha = 0.5$.

Figure 7. $\Psi - \eta$ curves calculated from Eq. (28) (stationary curves) and Eq. (13) (transient curves), calculated for different values of $\log(k_{d,macro}^0)$ (shown in the Figure). The transient curves have been calculated for the following values of $\xi_{s,lim}$: $\log(k_{d,macro}^0) = 2, 2.109$; $\log(k_{d,macro}^0) = 1, 1.698$; $\log(k_{d,macro}^0) = 0, 1.197$; $\log(k_{d,macro}^0) = -1, 1.091$; $\log(k_{d,macro}^0) = -2, 1.090$. $\alpha = 0.5$.

Figure 8. $\Psi - \eta$ (a) and $\eta - \ln(\Psi/1 - \Psi)$ (b) curves calculated from Eq. (28) (stationary curves, dashed-dotted lines) and Eq. (13) (transient curves, solid lines) calculated for $\log(k_{d,macro}^0) = -2$. The transient curves have been calculated for $\xi_{s,lim} = 1.090$. $\alpha = 0.5$

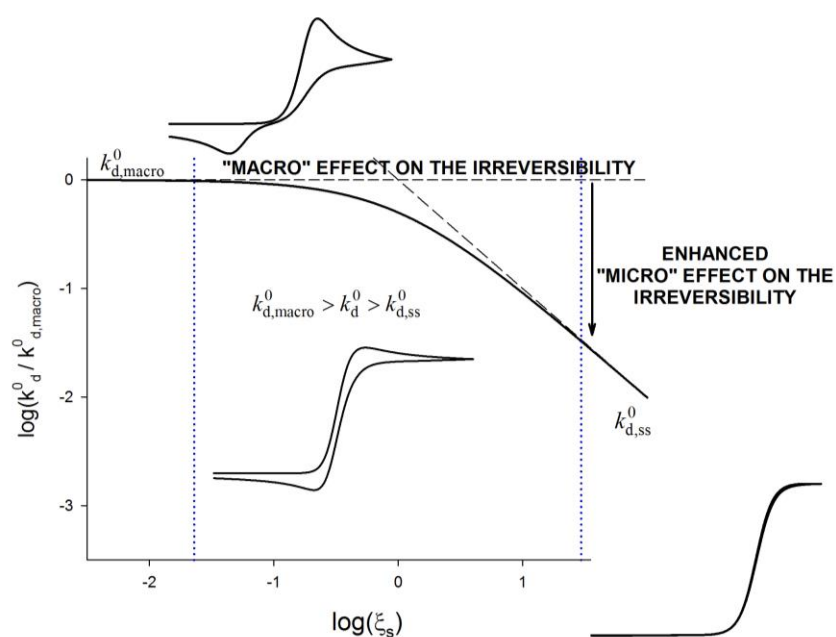
Figure B1. Influence of the electrode kinetics, through parameter $k_{d,macro}^0$ shown in the curves, on the dimensionless CV curves calculated for two values of ξ_s ($=1, 0.1$) indicated in the Figure. Solid and dashed lines correspond to analytical (Eq. (13)) numerical calculations (procedure discussed in refs. [39-41]), respectively. $\alpha = 0.5$.

Figure B2. Differences found between the analytical and numerical results for the peak potentials (a), half-peak potentials (b) and maximum currents (c) calculated by using Eq. (13) and the procedure discussed in refs. [39-41] for different values of $\log(\xi_s)$ shown in the curves. Figure B2d shows a zone diagram defining the values of $\log(\xi_s)$ and $\log(k_{d,macro}^0)$ for which the peak current / peak plateau calculated from Eq. (13) presents errors below 5%.

Scheme I. Region diagram of the peak / plateau currents. Vertical dashed lines indicate the value of $\log(\xi_s)$ for which a transition in the peak current / plateau current of the CV curves is taking place by assuming maximum differences of 5%.

Scheme II. Region diagram of the half-peak / half-wave potentials. Vertical dashed lines indicate the value of $\log(\xi_s)$ for which a transition in the values of the half-peak / half-wave potentials of the CV curves is taking place by assuming maximum differences of 5 mV.

Graphical abstract



Highlights

- An explicit analytical easily programmable expression for the current-potential curves of charge transfers of any degree of reversibility in Cyclic Voltammetry, valid for small spherical electrodes, is presented.
- A complete analysis of the most relevant parameters of the CV curves in terms of the electrode size and the scan rate is made
- The evolution of the main characteristics of the voltammograms in the transition from macro to microelectrodes is described.